

Elsevier required licence: © <2022>. This manuscript version is made available under the CC-BY-NC-ND 4.0 license <http://creativecommons.org/licenses/by-nc-nd/4.0/>  
The definitive publisher version is available online at [10.1016/j.apenergy.2022.119448](https://doi.org/10.1016/j.apenergy.2022.119448)

[Click here to view linked References](#)

# **A new shift mechanism for micro-explosion of water-diesel emulsion droplets at different ambient temperatures**

Zhaowen Wang <sup>a,b</sup>, Bo Yuan <sup>a,b</sup>, Junhui Cao <sup>a,b</sup>, Yuhang Huang <sup>c</sup>, Xiaobei Cheng <sup>a,b\*</sup>, Yuzhou  
Wang <sup>a,b</sup>, Xinhua Zhang <sup>a,b</sup>, Hao Liu <sup>a,b</sup>

<sup>a</sup> State Key Laboratory of Coal Combustion, Huazhong University of Science and Technology,  
Wuhan, 430074, China

<sup>b</sup> School of Energy and Power Engineering, Huazhong University of Science and Technology,  
Wuhan, 430074, China

<sup>c</sup> Centre for Green Technology, School of Civil and Environmental Engineering, University of  
Technology Sydney, 2007, NSW, Australia

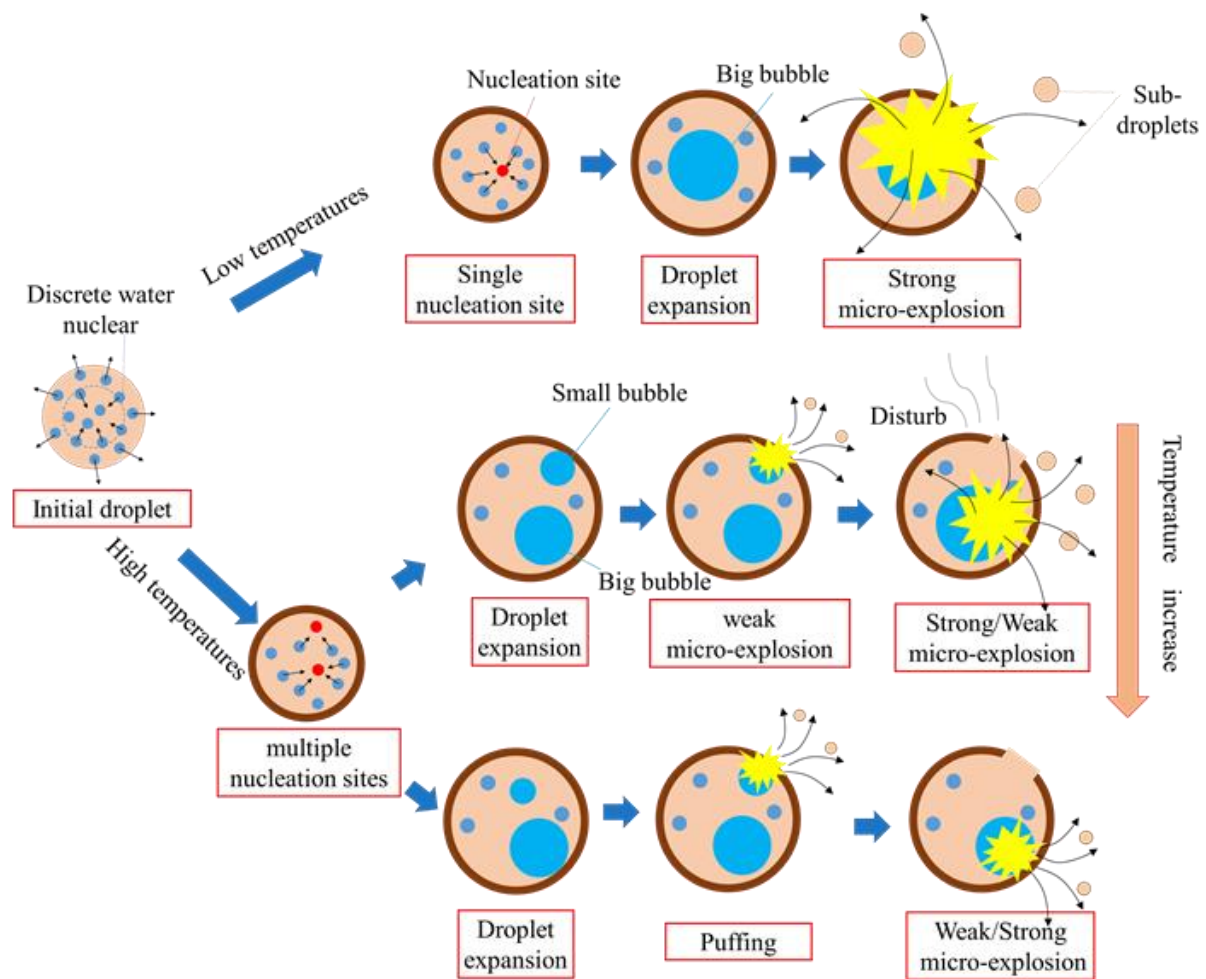
\* Corresponding author:

Prof Xiaobei Cheng, E-mail: [xbcheng@hust.edu.cn](mailto:xbcheng@hust.edu.cn)

## HIGHLIGHTS

- Bubble formation and micro-explosion modes of water emulsified diesel droplets were studied.
- Bubble nucleation changed from single site to multiple sites as ambient temperature increased.
- Bubble nucleation sites shifted from droplet center to surface as ambient temperature increased.
- Expansion intensity of droplet volume could describe the bubble formation process.
- Bubble formation and micro-explosion determined the evaporation behavior of fuel droplets.

## GRAPHICAL ABSTRACT



## Abstract

Water emulsified diesel is an ideal new alternative fuel for diesel engines, which has great potentials in reducing NO<sub>x</sub> and PM emissions simultaneously. A thorough understanding of its evaporation process is critical for achieving the emission reduction potentials. Therefore, this study investigated the evaporation characteristics of emulsion droplets with 65% diesel, 30% water and 5% surfactant by mass using the droplet suspension technology at ambient temperature 573-873 K. The normalized squared diameter, micro-explosion frequency, micro-explosion intensity and expansion intensity were used to quantify the effect of ambient temperature on the evaporation characteristics. The results showed that the evaporation process of water emulsified diesel droplets mainly included three stages, namely transient heating, fluctuation evaporation, and equilibrium evaporation. The maximum normalized squared diameter first increased with ambient temperature and then decreased, leading to a maximum of 2.91 at 773 K. The micro-explosion frequency first decreased and then increased, which was consistent with that of micro-explosion intensity. In addition, this study innovatively correlated the internal relationship between bubble formation and micro-explosion. Based on this, a new micro-explosion shift mechanism of water emulsified diesel droplets was proposed. As the ambient temperature increased, bubble nucleation in the droplet gradually changed from single site to multiple sites, and the nucleation sites shifted from the droplet center to surface.

**Keywords:** Water emulsified diesel; Droplet; Bubble nucleation; Micro-explosion; Shift mechanism

## 1. Introduction

The number of motor vehicles is increasing every year due to the rapid economic and population growths, which consumes a significant amount of fossil fuel and generates many pollutant emissions [1, 2]. Nitrogen oxides ( $\text{NO}_x$ ) and particulate matters (PM) are of the greatest concerns worldwide due to their serious adverse impacts on the environment and human health [3, 4]. Therefore, improving the emission performance and thermal efficiency has become a hot research topic for the internal combustion engine industry.

Water emulsified diesel is an oil-water mixture formed by adding a certain amount of water and a small amount of emulsifier to pure diesel through high-speed stirring, ultrasonic mixing, or other external forces. Water emulsified diesel is an ideal alternative fuel because the addition of water shifts the combustible range to higher fuel equivalence ratio side and consequently reduces emissions [5]. Firstly, in-cylinder temperature is reduced by water evaporation, which reduces  $\text{NO}_x$  emission [6]. Secondly, water can provide additional free radical to facilitate the oxidation of soot, thus reducing PM emission [7]. Thirdly, there is micro-explosion phenomenon in water emulsified diesel due to preferential evaporation of water, which breaks droplet and generates lots of smaller sub-droplets. This promotes fuel evaporation and air-fuel mixing, resulting in the improvement of thermal efficiency [8, 9]. Many researchers have verified the practical application potential of emulsified diesel in internal combustion engines [10, 11]. Maji et al. [12] studied the performance and emission characteristics of emulsified diesel in a single-cylinder engine. They found that the thermal efficiency of emulsified diesel remained almost unchanged while the fuel consumption rate was reduced. Khatri et al. [13] concluded that emulsified diesel could improve combustion and emission performance in diesel engines without any engine modification. Hassan et al. [14] and Mondal and Mandal [15] found that  $\text{NO}_x$  and smoke emissions were significantly reduced when using water emulsified diesel. Kumar et al. [16] prepared water-diesel emulsion with optimized process parameters and investigated its effect on the performance of a diesel engine. The results showed that the brake thermal efficiency was enhanced and  $\text{NO}_x$ , carbon monoxide and unburned hydrocarbon were reduced by 26.11%, 8.80% and 39.60%, respectively.

Proper fuel evaporation processes are of great importance for achieving the optimal engine performance. However, fuel evaporation especially micro-explosion [17] characteristics cannot be directly observed by using the engine test bench or constant volume chamber. Therefore, it is needed to investigate the evaporation characteristics of fuel droplets using other methods. Droplet levitation [18, 19], free-falling droplet [20, 21], and droplet suspension [22, 23]

technologies can be adopted to investigate the evaporation characteristics of a droplet. Among them, droplet levitation and free-falling droplet technologies can eliminate the influence of the thermocouple. However, the droplet is unstable during the evaporation process, which increases the difficulty in the visualization measurements and result analysis. In the droplet suspension technology, a droplet is suspended on a thermocouple node and transported into a hot environment. Although this technology causes some effect from the thermocouple, it is possible to obtain droplet inner temperature and images simultaneously. Especially, when the thermocouple diameter is less than 0.1 mm or the thermal conductivity is less than 80 W/m·K, the effect of heat transfer from the thermocouple can be ignored [24, 25]. Rehman et al. [26] concluded that the effect of thermocouple was ignorable when the ratio of the square of thermocouple diameter to the square of initial droplet diameter was less than 0.01. Wang et al. [27] also reported that the support had little impact on droplet evaporation when support size was less than 1/10 of droplet size. In addition, the heterogeneous nucleation arising from the thermocouple also has little influence on the occurrence of micro-explosion [28]. Thus, this technology is widely used for droplet micro-explosion.

Many scholars have experimentally studied the micro-explosion characteristics of emulsion droplets. Mura et al. [29] first studied the effect of the size of dispersed water droplets on micro-explosion of emulsion droplets and found that coalescence of dispersed water droplets had a positive effect on micro-explosion. Khan et al. [30] also pointed out that the aggregation process of discrete water nuclei and the size of the aggregated large water nuclei were determinants of micro-explosion generation for large droplets. Suzuki et al. [31] and Segawa et al. [32] found that micro-explosion generally occurred after water coalescence. The occurrence probability of micro-explosion could be improved by accelerating the aggregation and coalescence of dispersed water nuclei. Shen et al. [33, 34] observed the formation of single bubble at 433 K and pointed out that the break-up mode changed from catastrophic micro-explosion to local micro-explosion gradually in terms of probability as the ambient temperature increased. Avulapati et al. [35] observed the separation of emulsion constituents before micro-explosion at 773 K and found that the single nucleus of the separated component in the droplet resulted in more substantial explosion compared to multiple nuclei. Antonov et al. [36, 37] indicated that the smaller water nuclei inside the fuel droplet tended to merge and form fewer but larger water nuclei under the combustion of emulsion droplets. Similarly, Faik et al. [38] found different nucleation sites in water emulsified diesel droplets, and there was a phenomenon of bubbles merging during the combustion process.

Numerical simulations were also widely used to investigate bubble and micro-explosion of emulsion droplets. Scriven [39] formulated and simplified the equations of bubble growth in the nucleate boiling of binary mixtures to understand the processes of heat and mass transfer. Zeng and Chia-fon [40] developed a model in which a bubble was located in the droplet center and investigated the influences of composition, pressure and droplet size on micro-explosion. They found that micro-explosion was promoted by optimum composition and a certain level of high pressure. Girin [41] numerically studied the dynamics of micro-explosion of emulsified fuel droplets based on the assumption that a vapor bubble was surrounded by a fuel shell. They showed that perforation of fuel shell played an important role on micro-explosion and also calculated the number and the size of generated secondary droplets. Sazhin et al. [42] assumed that a water droplet was located in a fuel droplet and proposed a simple model to predict the puffing time or micro-explosion delay time of water-n-dodecane emulsion droplets. Fostiropoulos et al. [43, 44] further used a CFD model to predict the breakup time of water-heavy fuel emulsion droplets and confirmed that puffing was more efficient than aerodynamics in breaking droplet.

However, the above studies mainly focused on the quantitative analysis of the effect of parameters on micro-explosion and aggregation behavior before water evaporated or investigated specific aspects of emulsion droplet micro-explosion by numerical simulations. They rarely involved quantitative analysis of the effect of bubble generated by water evaporation on the micro-explosion modes and their shift mechanisms.

The droplet inner temperature of fuel spray in a practical engine varies in a wide range from low temperature before injection to high temperature after combustion starts. Meanwhile, the ambient temperature has a significant influence on the micro-explosion characteristics of droplets [22]. Thus, investigating droplet evaporation characteristics at different temperatures is of great importance for evaluating its impact on engine performance. Hashimoto et al. [45] studied the droplet lifetime and evaporation rate during the evaporation of palm methyl ester droplets from 473 to 873 K. They reported that the residue volume decreased with increasing ambient temperature, and no residue existed at 873 K. Han et al. [23] investigated the duration of evaporation phase and the maximum normalized diameter of ethanol-diesel-biodiesel droplets from 623 to 723 K. It was found that higher ambient temperature resulted in higher fluctuation frequency and larger amplitude of the droplet diameter expansion. Zhang et al. [46] studied evaporation duration, maximum normalized diameter, and temperature rise rate during the evaporation of butanol-hexadecane droplets from 638 to 738 K. Meng et al. [47]

investigated micro-explosion intensity of bio-diesel, RP-3 and ethanol mixed droplets at high temperatures, and divided the micro-explosion into slight, medium-intensity, strong and super micro-explosions according to micro-explosion intensity. Wang et al. [48] studied the droplet lifetime, micro-explosion delay time, and micro-explosion intensity during the evaporation of soybean oil droplets from 873 to 973 K. They implied that homogenous and heterogeneous nucleation led to strong and weak micro-explosion, respectively. Huang et al. [49] investigated evaporation rate, micro-explosion delay time, micro-explosion intensity of biodiesel/n-propanol blended droplets from 573 to 773 K. They indicated that the evaporation and micro-explosion characteristics of biodiesel/n-propanol droplets were closely related to the ambient temperature.

Previous studies mainly analyzed the effect of ambient temperature on evaporation processes of different fuel droplets, but did not explored the relationship between micro-explosion mode and ambient temperature, or the transition mechanism of micro-explosion modes. The aggregation process of water nuclei has great effect on the micro-explosion process. However, it can only be observed under low water content, large dispersed water nuclei size and specific temperature. Therefore, there is a lack of a universal method to analyze the micro-explosion modes at normal in-cylinder temperatures.

This study is therefore conducted to fill the above research gaps. The micro-explosion mechanism of water emulsified diesel droplets at 573-873 K is investigated in detail. The maximum normalized squared diameter, similarity and deformation degrees, micro-explosion frequency and intensity, and other parameters are used to quantitatively analyze the effect of ambient temperature on the evaporation characteristics of water emulsified diesel droplets. In particular, the relationship between micro-explosion mode and ambient temperature and then the transition mechanism of micro-explosion modes are explored. The main novelty is that this study proposes to use the expansion intensity as a new parameter to describe droplet expansion before micro-explosion occurs. Furthermore, a new analysis method is proposed by using the relationship between the expansion intensity and the micro-explosion intensity to analyze the micro-explosion modes at different temperatures, especially when the aggregation of water nuclei cannot be observed. Finally, an innovative micro-explosion mechanism diagram of emulsified diesel droplets is proposed for revealing the formation pattern of bubbles and the transition mechanism of micro-explosion modes at different ambient temperatures. The contribution of this study is to help better understand micro-explosion of emulsion droplets, which provides theoretical guidance for the practical application of emulsion fuels in engines



to improve engine performance.

## 2. Experimental apparatus and methods

### 2.1 Emulsion preparation

Micro-explosion of emulsion droplets is enhanced with the increase of water content. However, since water is not flammable and cannot provide any energy, engine power would decrease when there is too much water in emulsion fuel. Therefore, we chose a medium water mass ratio of 30% for the water emulsified diesel using commercial diesel from China National Petroleum Corporation. The surfactant combination is the most stable when the hydrophilic-lipophilic balance (HLB) is between 5-6 [50]. The components of the composite surfactant we used were Span 80, a non-ionic lipophilic surfactant with a HLB of 4.5 and Op10, a non-ionic hydrophilic surfactant with a HLB of 14.5. In this study, the composite surfactant with HLB of 5.26 was obtained by 99 g Span 80 and 8.14 g Op 10 (about 5%), which made emulsion more stable. The preparation process was as follows. Firstly, diesel and Span 80, and water and Op 10 were mixed according to the proportions, respectively. Then the mixed liquid was placed into the ultrasonic emulsifier (JP300G) for emulsification. The ultrasonic power, frequency, emulsification time, and motor speed were set to 500 W, 24 kHz, 30 min, and 100 r/min, respectively. Under these parameters, the size distribution of dispersed water droplets is shown in Fig. 1. As shown in Fig. 1, the numbers of small and large water droplets are less than that of medium water droplets. That is because water droplets cannot be counted if they are too small to observe. Therefore, the average particle size of the water droplets was 1.73  $\mu\text{m}$ , and the Sauter Mean Diameter (SMD) was 3.05  $\mu\text{m}$ . Through the above preparation method, the water emulsified diesel could be kept for at least 30 days without stratification, which met the requirement of the water emulsified diesel in this study.

### 2.2 Experimental apparatus

Fig. 2 shows the schematic of the experimental apparatus in this work. The experimental apparatus mainly includes three systems, namely droplet generation and transport system, heating and temperature control system, and visualization and image acquisition system. There

are two  $\varnothing 80$  mm quartz observation windows on the front and rear walls of the heating chamber. The top of the heating chamber has a 10 mm cylindrical hole for transferring an experimental droplet. A heating device is arranged in the inner cavity of the heating chamber. The droplet generation and transport system are used to generate a test droplet and deliver it to a high-temperature environment. Specifically, the experimental droplet with a diameter of 0.8-1.2 mm is produced by a microliter syringe. The droplet is suspended on a K-type thermocouple with a node diameter of 0.127 mm and then sent into the high-temperature chamber. To prevent the droplet from being heated in advance, a thermal baffle is installed between the droplet transport and heating systems. The heating system includes eight silicon nitride heating rods with a power of 600 W and a temperature control system adopts PID closed-loop control. The silicon nitride heating rods are evenly arranged in the circumferential direction to produce a uniform high-temperature environment. The temperature control system adjusts the power of the heating rod through the ambient temperature inside the constant volume combustion bomb cavity to achieve a precise control. The chamber can achieve a uniform temperature of 373-1200 K with an error of  $\pm 5$  K. The image acquisition is carried out with a high-speed CCD camera (IDT Motion Pro Y4-S1) and a LED lamp through the backlight method. The high-speed camera, jointly with a tele-macro lens (Nikon Micro-ED 200 mm f/4), achieves a full resolution of  $1024 \times 1024$  pixels at 2000 fps. More details about the test rig can be found in [46]. The experimental conditions are given in Table 1.

### 2.3 Digital image processing

Droplet diameter is a key parameter to evaluate the evaporation process, which is obtained by a MATLAB image processing code. Fig. 3 shows the procedures of image processing. Firstly, the image spatial resolution is obtained by calibrating the corundum tube. Secondly, the droplet area (ROI,  $300 \times 300$ ) is cut out from the original image ( $1024 \times 1024$ ) with the droplet at the center. Thirdly, the droplet and thermocouple are obtained through binarization using a proper threshold. Here, the threshold is dynamically adjusted according to the background brightness, and the connected domains are filled. After that, the droplet boundary is obtained by a 'bwboundaries' command. Then, the thermocouple width is fixed and the thermocouple is removed according to the change of boundary width. Finally, the droplet boundary can be extracted from the image.

The droplet squared diameter and normalized squared diameter are calculated by Eqs. (1)

and (2), respectively:

$$d^2 = 4 * N * \left(\frac{1}{l}\right)^2 / \pi \quad (1)$$

$$\text{Normalized squared diameter} = \frac{d^2}{d_0^2} \quad (2)$$

where  $d$  is the droplet diameter,  $d_0$  is the initial droplet diameter,  $N$  is the number of pixels of droplet projected area, and  $l$  is the image spatial resolution.

The similarity and deformation degrees are calculated by Eqs. (3) and (4), respectively [51]:

$$\text{Similarity Degree} = 100\% - \sqrt{\frac{\sum_{i,j}^{300 \times 300} (P_n(i,j) - P_{n+1}(i,j))^2}{300 \times 300}} \quad (3)$$

$$\text{Deformation Degree} = \frac{S_c}{S} = \frac{C^2}{4\pi S} \quad (4)$$

where  $P_n(i,j)$  represents the logical value 0 or 1 at  $(i,j)$  of the  $n^{\text{th}}$  image,  $P_{n+1}(i,j)$  represents the logical value 0 or 1 at  $(i,j)$  of the  $(n+1)^{\text{th}}$  image,  $S_c$  is the equivalent standard circle area calculated from the perimeter of the droplet projection,  $C$  is the perimeter of the actual droplet projection, and  $S$  is the droplet projected area.

## 2.4 Experimental uncertainties and errors

The droplet diameter and temperature during the evaporation are measured simultaneously. Table 2 lists the variables recorded and the systematic errors of measurement equipment. The normalization process can reduce the influence of error on the experimental results of droplet diameter and volume. The random errors mainly come from the distribution of discrete water phase in the initial droplets and the change in water sub-droplet location during the heating period [52]. Multiple experiments can reduce the random errors. In this study, ten experiments were repeated for each condition to reduce the random errors. The reported results in this article are the average values and the uncertainty is calculated by Eq. (5) [52]:

$$u = \sqrt{\frac{(x_1 - \bar{x})^2 + (x_2 - \bar{x})^2 + \dots + (x_n - \bar{x})^2}{n-1}} \quad (5)$$

where  $u$  is the uncertainty,  $x_1, x_2, \dots, x_n$  are experimental values,  $\bar{x}$  is the average value, and  $n$  is the number of effective experiments.

### 3. Results and discussion

#### 3.1 Evaporation process of water emulsified diesel droplet

Fig. 4 shows the variations of normalized squared diameter and liquid core temperature with time. Since the initial droplet diameters are different among experiments, this study utilizes the normalization of droplet diameter ( $d^2/d_0^2$ ) and the standardization of time ( $t/d_0^2$ ) to eliminate this influence, which is widely used in droplet experiments.

As shown in Fig. 4, the evaporation of water emulsified diesel includes three stages, which is same to that of other multi-component fuels [45, 53]. Specifically, stage (1) (before 0.480 s/mm<sup>2</sup>) is the transient heating, when the droplet diameter is almost equal to the initial diameter. Stage (2) (0.480-1.915 s/mm<sup>2</sup>) is the fluctuation evaporation when micro-explosion and puffing occur due to different evaporation rates of water and diesel, causing the droplet diameter to fluctuate drastically first and then slightly. In late stage (2),  $d^2/d_0^2$  increases due to bubble growth generated by a little water remained in droplet. Since pressure in the bubble is small, it cannot break the droplet. Stage (3) (1.915-3.766 s/mm<sup>2</sup>) is the equilibrium evaporation. In this stage,  $d^2/d_0^2$  of droplet decreases linearly and agrees with the  $d^2$  law. It is worth noting that there is a sudden decrease of the droplet diameter in late stage (3). This is because droplet surface tension decreases with the evaporation of oil film on droplet surface. The bubble ruptures when its pressure is higher than the sum of droplet surface tension and ambient pressure. Finally, after 3.766 s/mm<sup>2</sup>, the droplet image keeps nearly unchanged and is treated as the end of evaporation process. Due to the presence of gelatinous substance on the thermocouple [49], there are irregular and subtle fluctuations of droplet diameter.

Fig. 5 shows morphological changes during the evaporation of a water emulsified diesel droplet at 673 K. In Figs. 4 and 5, the droplet profile does not change until 0.480 s/mm<sup>2</sup>. On the one hand, the droplet expands due to heat absorption, leading to a gradual increase in diameter. On the other hand, the evaporation of diesel and water on the droplet surface reduces the droplet diameter. There is a dynamic balance between droplet expansion and surface evaporation, resulting in a constant droplet diameter.

From 0.480 to 0.511 s/mm<sup>2</sup>, the water vaporizes and generates bubbles. As the bubbles grow, the droplet profile gradually bulges and the diameter increases until the bubbles break the droplet at 0.511 s/mm<sup>2</sup>. After droplet fragmentation, its shape becomes irregular. The droplet regains its spherical shape at 0.516 s/mm<sup>2</sup> due to the surface tension. A complete micro-explosion cycle is completed from 0.480 to 0.516 s/mm<sup>2</sup>. After that, the droplet repeats the

processes of bubble generation, expansion, micro-explosion and shape recovery until 1.073 s/mm<sup>2</sup>, resulting in fluctuations of  $d^2/d_0^2$ . It is worth noting that the micro-explosion is different from the catastrophic micro-explosion of Shen et al. [54] and the total destruction of Moussa et al. [55, 56]. This is because the surfactant used in the experiment is composite and its amount is large, which increases the droplet surface tension and decreases the coalescence of water nuclei. Thus, the released energy by the sudden phase change of aggregated water droplet is insufficient to break the droplet. Then bubble generates and grows in the droplet. Since it takes a long time from formation to rapture, the bubble gradually shifts from the droplet center to the surface, resulting in incomplete droplet breakup [57]. Meanwhile, the characteristics of each micro-explosion are different. During 0.511-0.512 s/mm<sup>2</sup>, bubble nucleation occurs at the edge of the droplet where the surface tension is small. Thus, the droplet is broken before the bubble is fully expanded, and  $d^2/d_0^2$  is only 2.44. As the droplet heating continues, the water nuclei at different sites in the droplet agglomerate gradually as shown at 0.635 s/mm<sup>2</sup>, leading to an increased droplet volume and reaching a maximum  $d^2/d_0^2$  of 2.81. By 1.073 s/mm<sup>2</sup>, since the droplet has undergone multiple micro-explosions, the water content within the droplet is significantly reduced and cannot grow large bubbles. However, there are still many small water nuclei in the droplet that cannot agglomerate due to high Laplace pressure, which can be divided into three regions, as shown in Fig. 6 (a). Under the action of the flow inside the droplet, most water nuclei move to region I, where the surface tension is smaller. Then they evaporate and generate lots of small bubbles which are so easy to rapture that small sub-droplets are directly ejected from the droplet surface, causing slight fluctuations in the normalized droplet diameter, as shown in Fig. 6 (b). In region II, bubbles can grow larger and rapture when they overcome the surface tension, resulting in the formation of liquid column, whose tip splits and generates sub-droplets by Plateau-Rayleigh instability, as shown in Fig. 6 (c). Restricted by thicker oil film, the bubble generated by the evaporation of water nuclei in region III cannot break the droplet and only leads to the increase of droplet diameter in late stage (2), as shown in Fig. 6 (d).

After 1.915 s/mm<sup>2</sup>, the fluctuation evaporation phase ends and the droplet enters the equilibrium evaporation phase, as shown in Fig. 5. At this time, the evaporation is mainly for diesel. The  $d^2/d_0^2$  of droplet linearly decreases, and there is no apparent fluctuation in droplet shape except that the droplet instantly breaks when the oil film gradually evaporates to the surface of bubble generated in the late fluctuation evaporation phase at 3.153 and 3.154 s/mm<sup>2</sup>, which is called as passive rapture.

### 3.2 Similarity and deformation degrees

As defined by Eqs. (3) and (4) in section 2.3, the similarity degree reflects the instantaneous changes of droplet shape. A smaller similarity degree indicates a faster change of droplet shape. The deformation degree demonstrates the extent of deviation of droplet shape from the standard circle. As discussed in Section 3.1, the evaporation process of water emulsified diesel can be divided into three stages, i.e. transient heating, fluctuation evaporation, and equilibrium evaporation. However, the boundary between fluctuation and equilibrium evaporation is fuzzy. Zhang et al. [51] distinguished the evaporation process based on similarity and deformation degrees. Therefore, the present study divides the evaporation process into stages according to similarity and deformation degrees.

Fig. 7 provides similarity and deformation degrees at different ambient temperatures. As shown in Fig. 7, the similarity degree gradually increases in the early stage, which is attributed to the droplet oscillating due to droplet movement before it reaches the observation position. Then the evaporation process enters the transient heating stage, the similarity and deformation degrees remain unchanged. After that, the similarity degree decreases sharply, which means the start of the fluctuation evaporation stage. The similarity and deformation degrees remain almost unchanged in the equilibrium evaporation stage, except for small bumps. The small bumps should be the passive rupture according to Fig. 5. The ending time of fluctuation evaporation stage is defined as the last mutation time in similarity before the first passive rupture. When the equilibrium evaporation stage ends, the deformation degree rises sharply. In whole, there are many violent fluctuations in the similarity and deformation degrees, especially in the early stage of the fluctuation evaporation stage. Except that, the similarity degree is maintained at 96%-100% in the evaporation process.

The results in Fig. 7 indicate that the similarity of fluctuation evaporation stage sometimes recovers to over 96%, showing a multi-peak jagged structure at low temperatures. After each micro-explosion, the droplet attempted to return to a stable state and then starts the next micro-explosion. This could be explained by the fact that the droplet has sufficient time to absorb heat, expand, explode and recover at low temperatures. But at high temperatures, the fluctuation evaporation stage is shortened and the water in the droplet can quickly get a lot of energy to evaporate, which leads to the overlap of micro-explosions. Finally, as the temperature increases, the similarity curve changes from jagged to clustered distribution.

### 3.3 Normalized squared diameter and droplet inner temperature

The ambient temperature directly affects the heat absorption process of water emulsified diesel droplets, which determines the surfactant activity, water vaporization rate and nuclei aggregation. Therefore, the variation characteristics of droplet evaporation and inner temperature at different ambient temperatures are different. Fig. 8 displays the variations of normalized squared diameter and droplet inner temperature with time.

As shown in Fig. 8, the duration of transient heating stage gradually decreases as the ambient temperature increases. At 873 K, the heat transfer is extremely rapid and there is basically no transient heating stage. It indicates that the droplet heating mode gradually switches from a nearly infinite thermal conductivity mode (ICM) to a finite thermal conductivity mode (FCM) [58] as the ambient temperature increases. A larger temperature gradient leads to a faster heat transfer and a shorter dynamic equilibrium time for reaching a balance between droplet thermal expansion and surface evaporation rates. At low temperatures, the droplet gradually recovers after experiencing a micro-explosion cycle, and the recovered diameter is slightly smaller than that before expansion. While at high temperatures, the equivalent diameter of the recovered droplet after micro-explosion is gradually increasing. It implies that the water nuclei aggregation time is long at low temperatures, and the number of water nuclei aggregated at each time is small. There are no additional bubbles in the droplet after micro-explosion, leading to a reduced diameter. In contrast, multiple water nuclei vaporize simultaneously to produce bubbles at high temperatures. The bubbles remain in the droplets after each micro-explosion, resulting in a bigger droplet diameter than that before expansion. These characteristics will be described in detail in Section 3.4.

In the equilibrium evaporation stage, the evaporation rates of both diesel and water emulsified diesel increase with ambient temperature, as well as the difference between the evaporation rates of diesel ( $k$ ) and emulsified diesel ( $k_1$ ). Both  $k_1$  and  $k_2$  are the evaporation rates of emulsified diesel. The difference between  $k_1$  and  $k_2$  shows the evaporation rates before and after experiencing a passive rupture, which leads to less residual water inside the droplet. Therefore, the evaporation rate of emulsified diesel ( $k_2$ ) is closer to that of diesel ( $k$ ). The micro-explosion process is insufficient at high temperatures, resulting in more residual water inside the final droplet. Both the residual content and evaporation rate of water increase. Hence, when the ambient temperature increases from 573 to 773 K, the difference between the

1 evaporation rates of emulsified diesel (k1) and diesel (k) gradually increases from 0.038 mm<sup>2</sup>/s  
2 (equal to (-0.182 mm<sup>2</sup>/s)-(-0.144 mm<sup>2</sup>/s)) to 0.18 mm<sup>2</sup>/s. At 873 K, diesel droplets combust  
3 spontaneously and thus k value is unavailable.  
4

5  
6 Fig. 9 compares the droplet inner temperatures at different ambient temperatures. The  
7 droplet inner temperature exhibits a three-stage characteristic, including a linear rise, a quasi-  
8 stable stage and then another linearly rise. During the transient heating stage, the droplet  
9 temperature rise rate at each ambient temperature is approximately linear, which gradually  
10 increases from 66.4 to 215.4 K/(s/mm<sup>2</sup>) when ambient temperature is changed from 573 to 873  
11 K. Subsequently, due to the presence of water, some heat is absorbed by water to evaporate,  
12 resulting in a reduced growth rate of energy absorption and the droplet inner temperature enters  
13 the quasi-stable phase. When the ambient temperature gradually increases from 573 to 873 K,  
14 the times of entering the quasi-stable stage are 1.091, 0.512, 0.276, and 0.143 s/mm<sup>2</sup>,  
15 respectively. This indicates that a higher ambient temperature advances the quasi-stability phase.  
16 The first micro-explosion times are at 1.238, 0.508, 0.196, and 0.035 s/mm<sup>2</sup> comparing with  
17 Fig. 7, respectively. This means that the droplet inner temperature enters the quasi-steady state  
18 before the first micro-explosion in the low-temperature environment. The center and edge of  
19 the droplet reach the low boiling point temperature simultaneously, followed by the heat-  
20 absorbing vaporization of the water nucleus. However, the droplet inner temperature enters the  
21 quasi-steady state after the first micro-explosion moment at high temperatures, which implies  
22 that only the edge of the droplet has reached the low boiling point temperature and water  
23 vaporizes. In contrast, the center temperature has not yet reached the low boiling point  
24 temperature. It shows that the droplet is unevenly heated internally. This again proves that the  
25 heating mode at low temperatures is infinite thermal conductivity mode, where the droplet is  
26 uniformly heated and then generates bubbles. While the heating mode at high temperatures is a  
27 finite thermal conductivity mode, in which the water nucleus near the droplet surface is heated  
28 and vaporizes first before the temperature of droplet center reaches the water boiling point.  
29 After entering the quasi-stable stage, the temperature of the center remains almost constant at  
30 different ambient temperatures, which is slightly above the water boiling point. Hence, a certain  
31 superheat degree is acquired for the generation of micro-explosion.  
32  
33  
34  
35  
36  
37  
38  
39  
40  
41  
42  
43  
44  
45  
46  
47  
48  
49  
50  
51  
52

53  
54 Fig. 10 shows the effect of ambient temperature on the maximum normalized squared  
55 diameter  $((d^2/d_0^2)_{max})$ . The average values of  $(d^2/d_0^2)_{max}$  are 2.76, 2.84, 2.91 and 2.69 at  
56 573, 673, 773 and 873 K, respectively.  $(d^2/d_0^2)_{max}$  first increases and then decreases with  
57 ambient temperature. This may be because bubble nucleation in the droplet changes from single  
58  
59  
60  
61  
62  
63  
64  
65



site to multiple sites, and the expansion of each bubble decreases due to the influence of surface tension, which will be further discussed in section 3.4. Bubble generation process in the droplet includes two modes, i.e. single nucleation site and multiple nucleation sites. Single nucleation is dominant in the early stage of fluctuation evaporation stage at low temperatures. After a single bubble bursts, there are no other bubbles in the droplet and the droplet reverts to a spherical shape, which cannot form a cumulative effect. With the increase of temperature, the temperature transmission rate inside the droplet is fast, leading to the multiple nucleation site mode. The occurrence time of micro-explosion gradually advances, which reduces the time for water nuclei to gather. The droplet forms multiple water nuclei at different sites, which vaporize and explode sequentially. Then the droplet cannot fully recover, producing a cumulative effect in the droplet diameter. Therefore,  $(d^2/d_0^2)_{max}$  increases from 573 to 773 K. Higher temperature reduces the droplet surface tension and increases the probability of bubbles merging [38]. Therefore,  $(d^2/d_0^2)_{max}$  decreases when the ambient temperature exceeds 773 K.

### 3.4 Bubble formation and micro-explosion modes

Various definitions of micro-explosion intensity have been proposed. Some studies [59-61] used the ratio of expanded diameter before droplet breakup and initial diameter to characterize micro-explosion intensity. Zhang et al. [62] defined the micro-explosion intensity as the ratio between initial droplet diameter and diameter after micro-explosion, while Wang et al. [48] defined the micro-explosion intensity as the ratio of normalized squared diameters before and after micro-explosion. Since micro-explosion intensity indicates the capability of a droplet breaking into sub-droplets, Huang et al. [49] used the ratio of normalized squared diameter difference before and after droplet breakup to the normalized diameter after droplet breakup. In this study, the individual [49] and total [48] micro-explosion intensities are defined using Eqs. (6) and (7), respectively.

$$I = \frac{d_1^2}{d_2^2} \quad (6)$$

$$\text{Microexplosion intensity} = \sum_{i=0}^n \frac{d_{i1}^2}{d_{i2}^2} \quad (7)$$

where  $d_1$  and  $d_2$  are the diameters before and after droplet breakup, respectively;  $i1$  and  $i2$  stand for the start and end of each micro-explosion, respectively;  $n$  is the number of micro-explosion including both strong and weak micro-explosions. Table 3 shows the classification criteria for micro-explosion intensity in this study.

Figs. 11 and 12 show the micro-explosion frequency and intensity at various ambient temperatures, respectively. The micro-explosion frequency is the number of micro-explosion during the whole evaporation process. As shown in Figs. 11 and 12, the percentage of weak micro-explosions is significantly more than strong micro-explosions. Both strong and weak micro-explosion frequencies decrease first and then increase with the ambient temperature. Micro-explosion intensity and frequency demonstrate the same variation trends, which implies that the micro-explosion mode changes when the ambient temperature gradually increases from 573 to 873 K. To explore the shift mechanisms of droplet micro-explosion at different temperatures, this study innovatively investigates individual bubble's formation characteristics and correlates bubble formation with micro-explosion.

An initial deduction can be inferred as follows based on the above analysis and results from other researchers [63, 64]. When the ambient temperature rises from 573 to 773 K, the time for water nuclei agglomeration reduces gradually due to the improvement of heat transfer. Therefore, water nuclei near the droplet surface have no time to participate in the agglomeration of water nuclei inside the droplet and evaporate directly and generate bubbles. This makes bubble generation change from single nucleation site to multiple nucleation sites gradually, while the expansion of each bubble decreases accordingly. At the same time, the bubbles cannot merge since the bubble number is small and bubbles are far apart. As a result, some strong micro-explosions become weak micro-explosions, and weak micro-explosions become puffing. With the further increase of ambient temperature to 873 K, heat transfer in fuel droplet is further intensified. It increases the number and growth rate of bubbles and decreases diesel viscosity, which improve the probability for smaller bubbles merging into larger bubbles under the action of pressure difference between bubbles [36, 51, 65]. This causes partial conversion of puffing to weak micro-explosion and weak micro-explosion to strong micro-explosion. Eventually, the micro-explosion frequency and intensity increase at 873 K.

To verify the above deduction, this study investigates the bubble generation characteristics. Specifically, an expansion intensity ( $EI$ ) is proposed to describe the expansion degree before droplet fragmentation, as defined in Eq. (8).

$$EI = \frac{d_3^2}{d_2^2} \quad (8)$$

where  $d_2$  is the diameter after droplet breakup and  $d_3$  is the diameter before the next breakup. This study concludes that  $EI > 1.4$  can better characterize the generation process of a bubble. This threshold value classifies weak and strong micro-explosions, and then facilitates

the study on shift mode of micro-explosion.

Fig. 13 shows the bubble formation and micro-explosion characteristics at different ambient temperatures. The percentage of lifetime span means the occurrence moment of each micro-explosion compared to the total droplet evaporation lifetime. At 573 K, strong micro-explosions almost always coincide with bubble formation. It indicates that water nuclei at low temperatures gather in the center and evaporate to form a bubble, followed by strong or weak micro-explosions instantaneously when the diameter reaches its peak. At 673 K, a small part of the bubble formation process coincides with the strong micro-explosion, and most of it coincides with weak micro-explosion process. At 773 K, the bubble formation process mainly coincides with weak micro-explosion. It indicates that the water nuclei begin accumulate at multiple sites inside the droplet and the expansion process is caused by the joint expansion of multiple bubbles as the ambient temperature increases. While the rapture of single bubble causes a slight decrease in droplet diameter, the final bubble formation often be interrupted and coincides with the weak micro-explosion process. Eventually, the bubble formation process is separated from both strong and weak micro-explosions when the temperature is further increased to 873 K. It indicates that droplet expansion is interrupted by puffing, resulting in an increase of minor droplet diameter. The bubble formation process coincides with the puffing process. It is also clear from Fig. 13 that the number of bubble formation processes ( $EI > 1.4$ ) gradually decreases with the increase of ambient temperature. It means that the bubbles are first generated at the droplet edge at high temperatures and causes more small bubbles to break up by puffing, resulting in a smaller expansion intensity of each expansion process than the threshold.

The micro-explosion mechanism of water emulsified diesel droplets at different ambient temperatures is shown in Fig. 14 based on the relationship between bubble formation and micro-explosion intensity. At low temperatures, bubble formation is dominated by single-site nucleation, which leads to the formation of a big bubble. The bubble expands sufficiently to cause strong micro-explosion [35]. At high temperatures, bubble formation is dominated by multi-site nucleation, which leads to two phenomena, i.e. 1) weak and strong/weak micro-explosion occurring sequentially, or 2) puffing and weak/strong micro-explosion occurring sequentially.

Fig. 15 specifically compares bubble nucleation and droplet micro-explosion at different ambient temperatures. The images are used to further verify the micro-explosion mechanism in Fig. 14. Yellow circles indicate droplet breakup positions, and red, black and blue boxes

indicate bubble formation, strong micro-explosions, and weak micro-explosions, respectively. When the end of bubble formation and the beginning of micro-explosion overlap, which are indicated as “○” and “Δ” or “■” coincide in Fig. 13. At 573 K, the droplet expands from the first to fourth picture, and its shape is close to a circle. The broken droplet’s diameter is smaller than that before the expansion, which means that there is only one bubble inside the droplet. The single-site nucleation at a low temperature produces only one big bubble and forms a strong micro-explosion. As the ambient temperature increases to 673 K, the bubble formation mode is significantly diversified. The droplet temperature is uneven at high temperatures. Therefore, the droplet edge is preferentially heated to form single site nucleation, causing a strong micro-explosion, as shown in the upper column of 673 K in Fig. 15. In addition, there are some cases of multi-site nucleation, where multiple bubbles expand together, as shown in the bottom column of 673 K in Fig. 15. When the ambient temperature increases to 773 K, multiple bubbles expand together. The droplet expands from the first to third image, forming two clear bubbles at upper and bottom edge of the droplet and reaching the maximum droplet diameter. The bubble at the bottom of the edge then breaks the droplet, and a weak micro-explosion occurs. The formation of bubbles, in this case, is multi-site nucleation and bubble formation mostly coincides with weak micro-explosion. When the ambient temperature reaches 873 K, large bubbles are generated inside the droplet, and micro-explosion occurs after expansion (fourth image). However, puffing (second image) and small micro-explosion also occur several times in the edge region. It indicates that after bubble generation, puffing leads to the bubble formation separated from both strong and weak micro-explosion processes due to the intense surface disturbance.

In summary, the droplet has enough time to gather water nuclei and form an extensive water nucleus at low temperatures. Due to large temperature gradient inside the droplet, multiple water nuclei evaporate simultaneously at high temperatures. The droplet nucleation gradually changes from single site to multiple sites and the bubble nucleation sites gradually shift from the droplet center to surface as the ambient temperature increases, resulting in the transition from the coincidence of bubble formation with strong micro-explosion to with weak micro-explosion. Finally, the bubble formation process separates from both strong and weak micro-explosions.

#### 4. Conclusion

Evaporation and micro-explosion characteristics of water-diesel emulsion droplets with 30% water content were investigated using the droplet suspension technology at ambient temperature 573 K, 673 K, 773 K and 873 K. The normalized squared diameter, droplet inner temperature, micro-explosion intensity and frequency, and expansion intensity were discussed. Then this study innovatively correlated bubble formation with micro-explosion to explore the micro-explosion modes of water emulsified diesel droplets at different ambient temperatures. The main conclusions of the present study can be drawn as follows:

(1) The evaporation process of water emulsified diesel droplets mainly includes three stages, namely transient heating, fluctuation evaporation and equilibrium evaporation.

(2) Due to the cumulative effect of bubbles, the maximum normalized squared diameter of the droplet first increases to the peak at 773 K and then decreases with further increase of ambient temperature.

(3) With the increase of ambient temperature, bubble nucleation in the droplet gradually changes from single site to multiple sites, and the bubble nucleation sites gradually shift from the droplet center to surface.

(4) With the increase of ambient temperature, total micro-explosion intensity decreases first and then increases due to the shifts of bubble formation and micro-explosion mode.

(5) The coincident relationship between bubble formation and micro-explosion can determine the explosion mode and the micro-explosion intensity of diesel-water emulsion droplets.

In the future, the work should focus on the visualization of bubble and bubble motion in emulsion droplets, especially quantitative research. Further, this study was conducted at atmospheric pressure, which was lower than diesel engine operation pressure. The micro-explosion at high pressure should be investigated. Finally, although the effect of thermocouple may be small, developing advanced models is an effective way to eliminate the disturbance of a foreign part and to investigate micron emulsion droplets which are the spray droplet sizes in real engines.

## Acknowledgments

This work was supported by the National Natural Science Foundation of China (Grant

number 51576083). The assistance of Hao Chi, Huimin Wu, and Yu Zhang in the experiments is greatly appreciated. The fourth author Y.H. is a recipient of the ARC Discovery Early Career Research Award (DE220100552).

## References

- [1] Yi W, Yan J. Energy consumption and emission influences from shared mobility in China: A national level annual data analysis. *Appl Energy* 2020;277:115549.
- [2] Lane B, Shaffer B, Samuelsen S. A comparison of alternative vehicle fueling infrastructure scenarios. *Appl Energy* 2020;259:114128.
- [3] Huang Y, Lee CKC, Yam Y-S, Mok W-C, Zhou JL, Zhuang Y, Surawski NC, Organ B, Chan EFC. Rapid detection of high-emitting vehicles by on-road remote sensing technology improves urban air quality. *Sci Adv* 2022;8(5):eabl7575.
- [4] Huang Y, Lei C, Liu CH, Perez P, Forehead H, Kong S, Zhou JL. A review of strategies for mitigating roadside air pollution in urban street canyons. *Environ Pollut* 2021;280:116971.
- [5] Park S, Woo S, Kim H, Lee K. The characteristic of spray using diesel water emulsified fuel in a diesel engine. *Appl Energy* 2016;176:209-20.
- [6] Xu Y, Hellier P, Purton S, Baganz F, Ladommatos N. Algal biomass and diesel emulsions: An alternative approach for utilizing the energy content of microalgal biomass in diesel engines. *Appl Energy* 2016;172:80-95.
- [7] Debnath BK, Saha UK, Sahoo N. A comprehensive review on the application of emulsions as an alternative fuel for diesel engines. *Renew Sust Energ Rev* 2015;42:196-211.
- [8] Daho T, Vaitilingom G, Ouiminga SK, Piriou B, Zongo AS, Ouoba S, Koulidiati J. Influence of engine load and fuel droplet size on performance of a CI engine fueled with cottonseed oil and its blends with diesel fuel. *Appl Energy* 2013;111:1046-53.
- [9] Ismael MA, Heikal MR, Aziz ARA, Syah F, Zainal A EZ, Crua C. The effect of fuel injection equipment on the dispersed phase of water-in-diesel emulsions. *Appl Energy* 2018;222:762-71.
- [10] Sidhu MS, Roy MM, Wang W. Glycerine emulsions of diesel-biodiesel blends and their performance and emissions in a diesel engine. *Appl Energy* 2018;230:148-59.
- [11] Ogunkoya D, Li S, Rojas OJ, Fang T. Performance, combustion, and emissions in a diesel engine operated with fuel-in-water emulsions based on lignin. *Appl Energy* 2015;154:851-61.
- [12] Maji D, Mondal P, Kumar Mandal B. Experimental investigation on the use of water emulsified diesel in a single cylinder Compression Ignition engine. *IOP Conference Series: Materials Science and Engineering* 2018;377:012123.
- [13] Khatri D, Goyal R. Performance, emission and combustion characteristics of water diesel emulsified fuel for diesel engine: A review. *Mater Today: Proc* 2020;28:2275-8.
- [14] Hassan ZU, Usman M, Asim M, Kazim AH, Farooq M, Umair M, Imtiaz MU, Asim SS. Use of diesel and emulsified diesel in CI engine: A comparative analysis of engine characteristics. *Sci Prog* 2021;104(2):1-19.
- [15] Mondal PK, Mandal BK. A comparative study on the performance and emissions from a CI engine fuelled with water emulsified diesel prepared by mechanical homogenization and ultrasonic dispersion method. *Energy Rep* 2019;5:639-48.
- [16] Kumar N, Raheman H, Machavaram R. Performance of a diesel engine with water emulsified diesel

- prepared with optimized process parameters. *Int J Green Energy* 2019;16(9):687-701.
- [17] Wang Z, Shi S, Huang S, Tang J, Du T, Cheng X, Huang R, Chen J-Y. Effects of water content on evaporation and combustion characteristics of water emulsified diesel spray. *Appl Energy* 2018;226:397-407.
  - [18] Chaitanya Kumar Rao D, Basu S. Phenomenology of disruptive breakup mechanism of a levitated evaporating emulsion droplet. *Exp Therm Fluid Sci* 2020;115:110086.
  - [19] Junk M, Hinrichs J, Polt F, Fechner J, Pauer W. Quantitative experimental determination of evaporation influencing factors in single droplet levitation. *Int J Heat Mass Transf* 2020;149:119057.
  - [20] Jang GM, Kim NI. Characteristics of a free-falling single-droplet of water-in-oil emulsion broken up by a pulse laser. *Fuel* 2020;264:116863.
  - [21] Sultana KR, Pope K, Lam LS, Muzychka YS. Phase change and droplet dynamics for a free falling water droplet. *Int J Heat Mass Transf* 2017;115:461-70.
  - [22] Kim H, Won J, Baek SW. Evaporation of a single emulsion fuel droplet in elevated temperature and pressure conditions. *Fuel* 2018;226:172-80.
  - [23] Han K, Zhao C, Fu G, Zhang F, Pang S, Li Y. Evaporation characteristics of dual component droplet of benzyl azides-hexadecane mixtures at elevated temperatures. *Fuel* 2015;157(270-278):270-8.
  - [24] Harada T, Watanabe H, Suzuki Y, Kamata H, Matsushita Y, Aoki H, Miura T. A numerical investigation of evaporation characteristics of a fuel droplet suspended from a thermocouple. *Int J Heat Mass Transf* 2011;54(1-3):649-55.
  - [25] Wang J, Huang X, Qiao X, Ju D, Sun C. Experimental study on effect of support fiber on fuel droplet vaporization at high temperatures. *Fuel* 2020;268:117407.
  - [26] Rehman HL-u, Weiss J, Seers P. Effect of heat conduction on droplet life time and evaporation rate under forced convection at low temperatures. *Exp Therm Fluid Sci* 2016;72:59-66.
  - [27] Wang Z, Yuan B, Huang Y, Cao J, Wang Y, Cheng X. Progress in experimental investigations on evaporation characteristics of a fuel droplet. *Fuel Process Technol* 2022;231:107243.
  - [28] Mura E, Massoli P, Josset C, Loubar K, Bellettre J. Study of the micro-explosion temperature of water in oil emulsion droplets during the Leidenfrost effect. *Exp Therm Fluid Sci* 2012;43:63-70.
  - [29] Mura E, Josset C, Loubar K, Huchet G, Bellettre J. Effect of dispersed water droplet size in microexplosion phenomenon for water in oil emulsion. *Atomization spray* 2010;20(9):791-9.
  - [30] Yahaya Khan M, Abdul Karim ZA, Aziz ARA, Heikal MR, Crua C. Puffing and Microexplosion Behavior of Water in Pure Diesel Emulsion Droplets During Leidenfrost Effect. *Combust Sci Technol* 2016;189(7):1186-97.
  - [31] Suzuki Y, Harada T, Watanabe H, Shoji M, Matsushita Y, Aoki H, Miura T. Visualization of aggregation process of dispersed water droplets and the effect of aggregation on secondary atomization of emulsified fuel droplets. *Proc Combust Inst* 2011;33(2):2063-70.
  - [32] Segawa D, Yamasaki H, Kadota T, Tanaka H, Enomoto H, Tsue M. Water-coalescence in an oil-in-water emulsion droplet burning under microgravity. *Proc Combust Inst* 2000;28(1):985-90.
  - [33] Shen S, Che Z, Wang T, Yue Z, Sun K, Som S. A model for droplet heating and evaporation of water-in-oil emulsified fuel. *Fuel* 2020;266:116710.
  - [34] Shen S, Sun K, Che Z, Wang T, Jia M, Cai J. An experimental investigation of the heating behaviors of droplets of emulsified fuels at high temperature. *Appl Therm Eng* 2019;161:114059.
  - [35] Avulapati MM, Megaritis T, Xia J, Ganippa L. Experimental understanding on the dynamics of micro-explosion and puffing in ternary emulsion droplets. *Fuel* 2019;239:1284-92.
  - [36] Antonov DV, Piskunov MV, Strizhak PA. Explosive disintegration of two-component drops under intense conductive, convective, and radiant heating. *Appl Therm Eng* 2019;152:409-19.

- [37] Antonov DV, Fedorenko RM, Strizhak PA, Castanet G, Sazhin SS. Puffing/micro-explosion of two closely spaced composite droplets in tandem: Experimental results and modelling. *Int J Heat Mass Transf* 2021;176:121449.
- [38] Faik AM-D, Zhang Y. Multicomponent fuel droplet combustion investigation using magnified high speed backlighting and shadowgraph imaging. *Fuel* 2018;221:89-109.
- [39] Scriven LE. On the dynamics of phase growth. *Chem Eng Sci* 1959;10(1-2):1-13.
- [40] Zeng Y, Chia-fon FL. Modeling droplet breakup processes under micro-explosion conditions. *Proc Combust Inst* 2007;31(2):2185-93.
- [41] Girin OG. Dynamics of the emulsified fuel drop microexplosion. *Atomization spray* 2017;27(5):407-22.
- [42] Sazhin SS, Rybdylova O, Crua C, Heikal M, Ismael MA, Nissar Z, Aziz ARBA. A simple model for puffing/micro-explosions in water-fuel emulsion droplets. *Int J Heat Mass Transf* 2019;131:815-21.
- [43] Fostiropoulos S, Strotos G, Nikolopoulos N, Gavaises M. A simple model for breakup time prediction of water-heavy fuel oil emulsion droplets. *Int J Heat Mass Transf* 2021;164:120581.
- [44] Fostiropoulos S, Strotos G, Nikolopoulos N, Gavaises M. Numerical investigation of heavy fuel oil droplet breakup enhancement with water emulsions. *Fuel* 2020;278:118381.
- [45] Hashimoto N, Nomura H, Suzuki M, Matsumoto T, Nishida H, Ozawa Y. Evaporation characteristics of a palm methyl ester droplet at high ambient temperatures. *Fuel* 2015;143:202-10.
- [46] Zhang Y, Huang R, Wang Z, Xu S, Huang S, Ma Y. Experimental study on puffing characteristics of biodiesel-butanol droplet. *Fuel* 2017;191:454-62.
- [47] Meng K, Fu W, Lei Y, Zhao D, Lin Q, Wang G. Study on micro-explosion intensity characteristics of biodiesel, RP-3 and ethanol mixed droplets. *Fuel* 2019;256:115942.
- [48] Wang L, Wang J, Qiao X, Ju D, Lin Z. Effect of ambient temperature on the micro-explosion characteristics of soybean oil droplet: The phenomenon of evaporation induced vapor cloud. *Int J Heat Mass Transf* 2019;139:736-46.
- [49] Huang X, Wang J, Wang Y, Qiao X, Ju D, Sun C, Zhang Q. Experimental study on evaporation and micro-explosion characteristics of biodiesel/n-propanol blended droplet. *Energy* 2020;205:118031.
- [50] Huo M, Lin S, Liu H, Lee C-ff. Study on the spray and combustion characteristics of water-emulsified diesel. *Fuel* 2014;123:218-29.
- [51] Zhang Y, Huang R, Xu S, Huang Y, Huang S, Ma Y, Wang Z. The effect of different n-butanol-fatty acid methyl esters (FAME) blends on puffing characteristics. *Fuel* 2017;208:30-40.
- [52] Antonov DV, Fedorenko RM, Strizhak PA, Nissar Z, Sazhin SS. Puffing/micro-explosion in composite fuel/water droplets heated in flames. *Combust Flame* 2021;233:111599.
- [53] Ma X, Zhang F, Han K, Yang B, Song G. Evaporation characteristics of acetone-butanol-ethanol and diesel blends droplets at high ambient temperatures. *Fuel* 2015;160:43-9.
- [54] Shen S, Sun K, Che Z, Wang T, Jia M, Cai J. Mechanism of micro-explosion of water-in-oil emulsified fuel droplet and its effect on soot generation. *Energy* 2020;191:116488.
- [55] Moussa O, Tarlet D, Massoli P, Bellettre J. Investigation on the conditions leading to the micro-explosion of emulsified fuel droplet using two colors LIF method. *Exp Therm Fluid Sci* 2020;116:110106.
- [56] Moussa O, Francelino D, Tarlet D, Massoli P, Bellettre J. Insight of a water-in-oil emulsion drop under leidenfrost heating using laser-induced fluorescence optical diagnostics. *Atomization spray* 2019;29(1):1-17.
- [57] Meng K, Han K, Li F, Bao L, Wang C, Lin Q. Study on combustion and micro-explosion characteristics of biodiesel and ethanol mixture droplets under different oxygen concentrations and temperatures. *Phys Fluids* 2021;33(5):052003.
- [58] Law CK, Sirignano WA. Unsteady droplet combustion with droplet heating—II: conduction limit.



Combust Flame 1977;28:175-86.

- [59] Wang CH, Hung WG, Fu SY, Huang WC, Law CK. On the burning and microexplosion of collision-generated two-component droplets: miscible fuels. Combust Flame 2003;134(3):289-300.
- [60] Botero ML, Huang Y, Zhu DL, Molina A, Law CK. Synergistic combustion of droplets of ethanol, diesel and biodiesel mixtures. Fuel 2012;94:342-7.
- [61] Hoxie A, Schoo R, Braden J. Microexplosive combustion behavior of blended soybean oil and butanol droplets. Fuel 2014;120:22-9.
- [62] Zhang X, Li T, Wang B, Wei Y. Superheat limit and micro-explosion in droplets of hydrous ethanol-diesel emulsions at atmospheric pressure and diesel-like conditions. Energy 2018;154:535-43.
- [63] Antonov DV, Nyashina GS, Strizhak PA, Romanov DS. Micro-explosive droplet fragmentation of environmentally promising coal-water slurries containing petrochemicals. Fuel 2021;283:118949.
- [64] Xi X, Liu H, Cai C, Jia M, Ma X. Analytical and experimental study on boiling vaporization and multi-mode breakup of binary fuel droplet. Int J Heat Mass Transf 2021;165:120620.
- [65] Stevenson P. Inter-bubble gas diffusion in liquid foam. Curr Opin Colloid Interface Sci 2010;15(5):374-81.

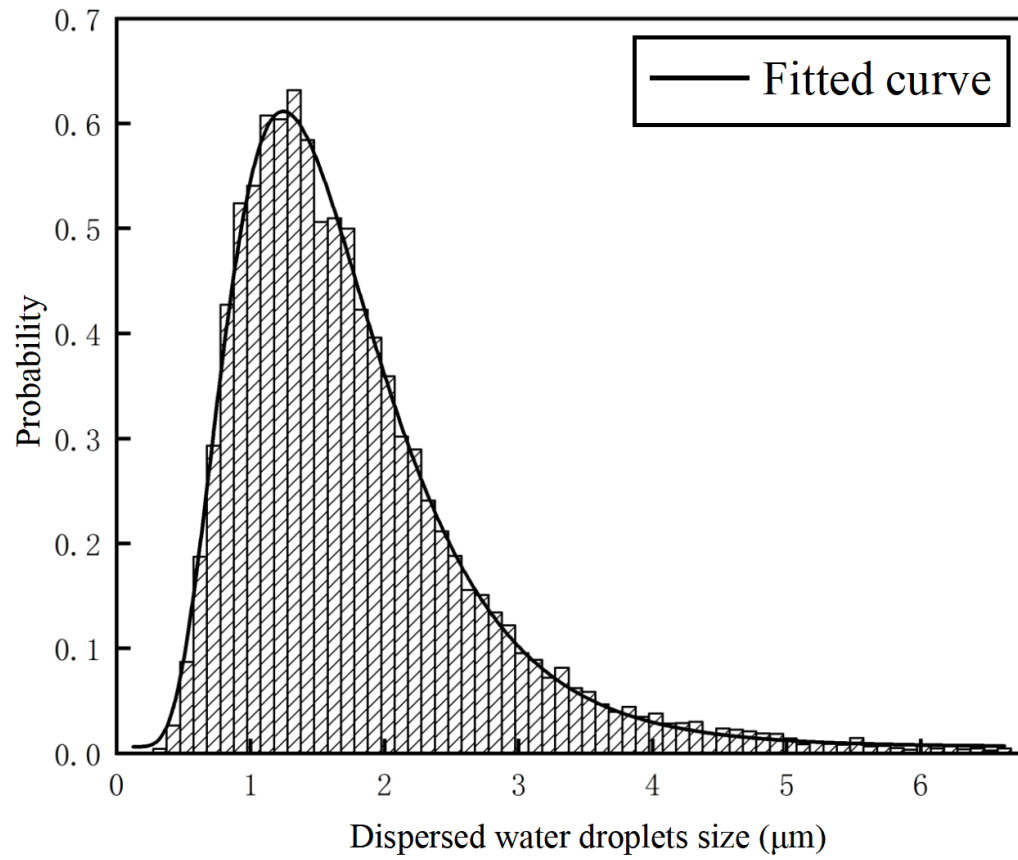


Fig. 1. The size distribution of dispersed water droplets in emulsion droplet.

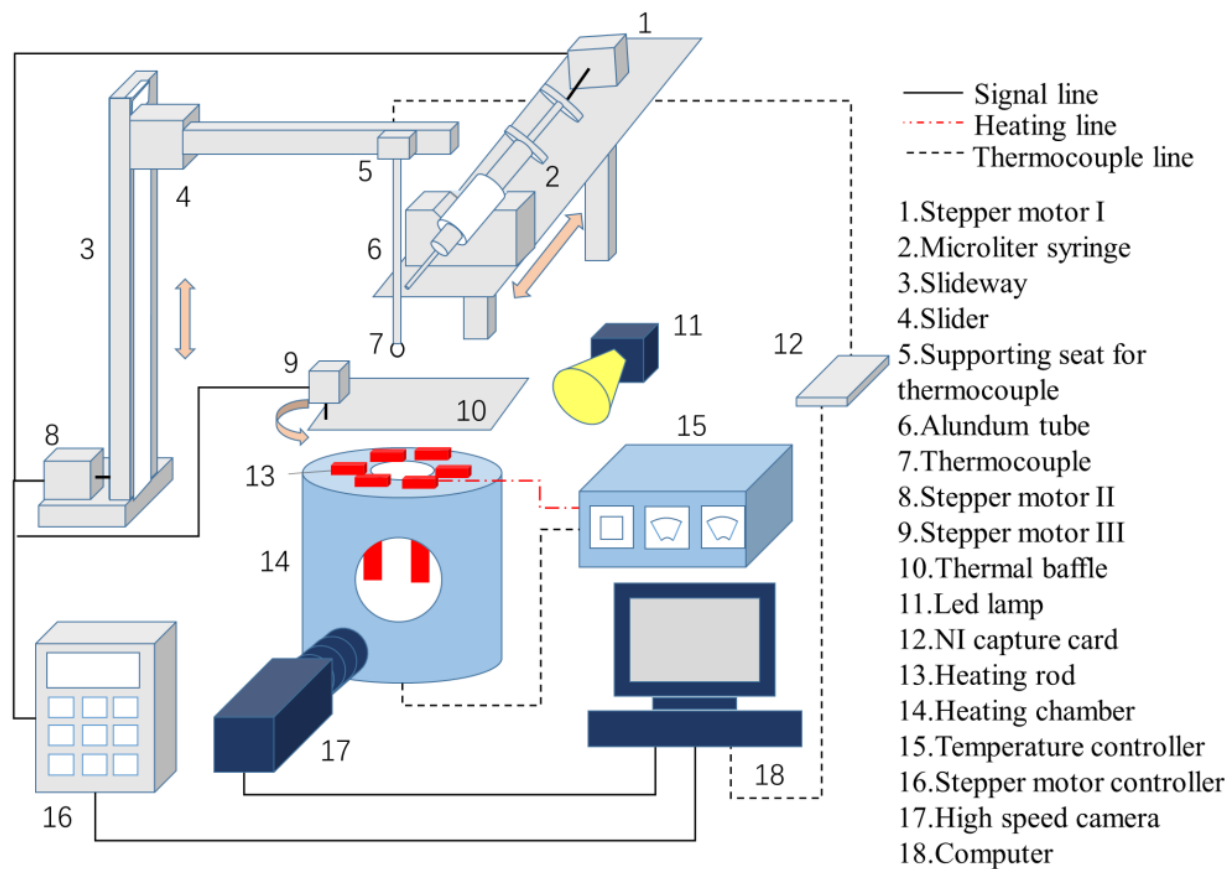


Fig. 2. Schematic of the experimental apparatus.

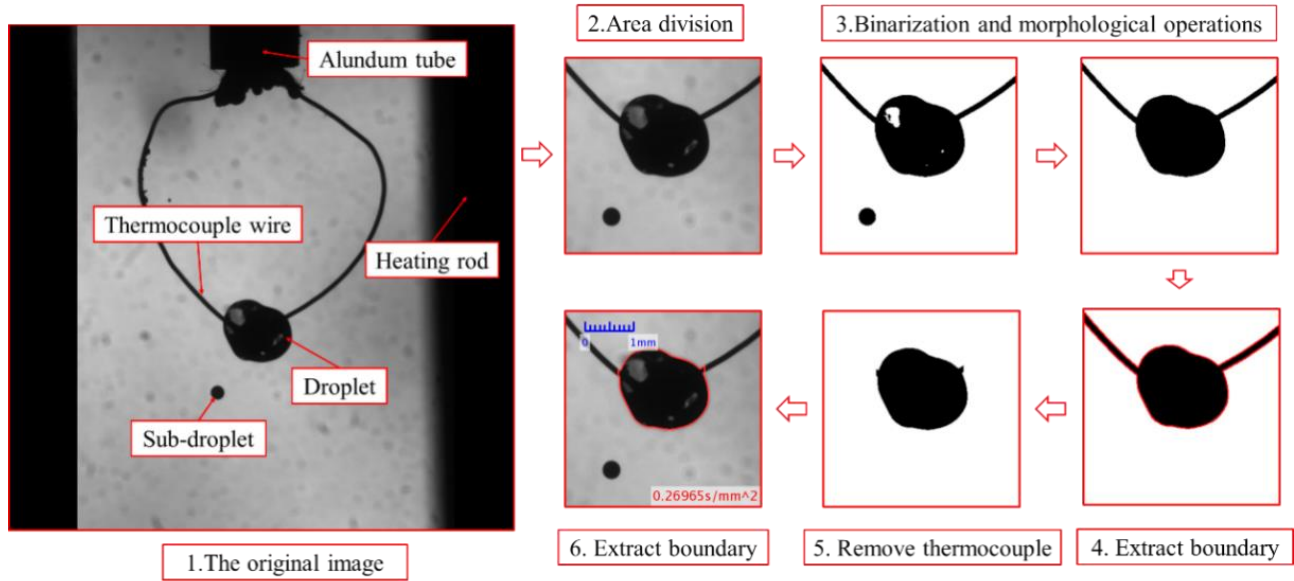


Fig. 3. Procedures of image processing.

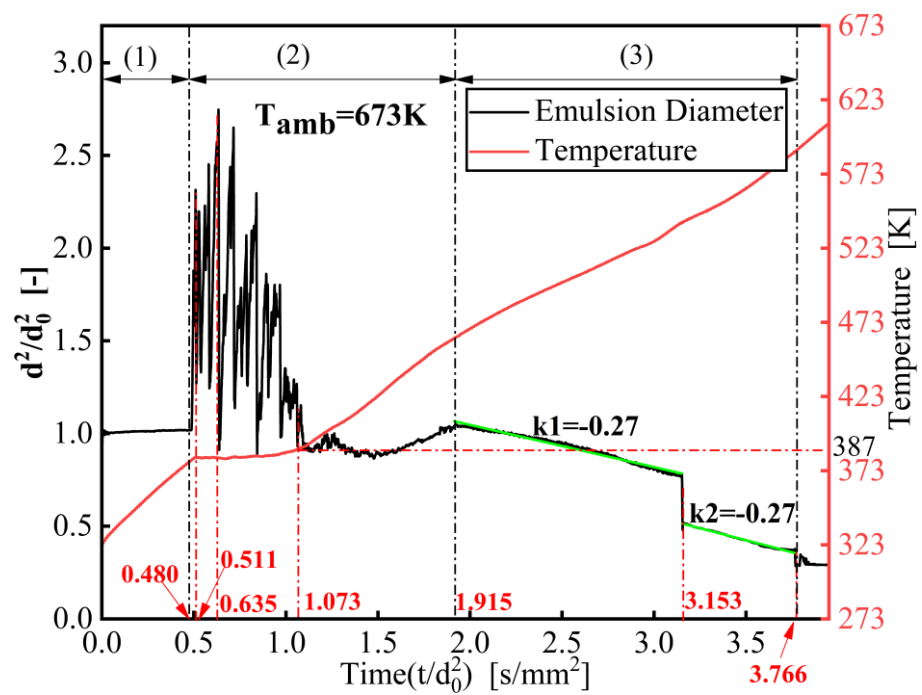


Fig. 4. Variations of normalized squared diameter ( $d^2/d_0^2$ ) and droplet inner temperature at 673 K.

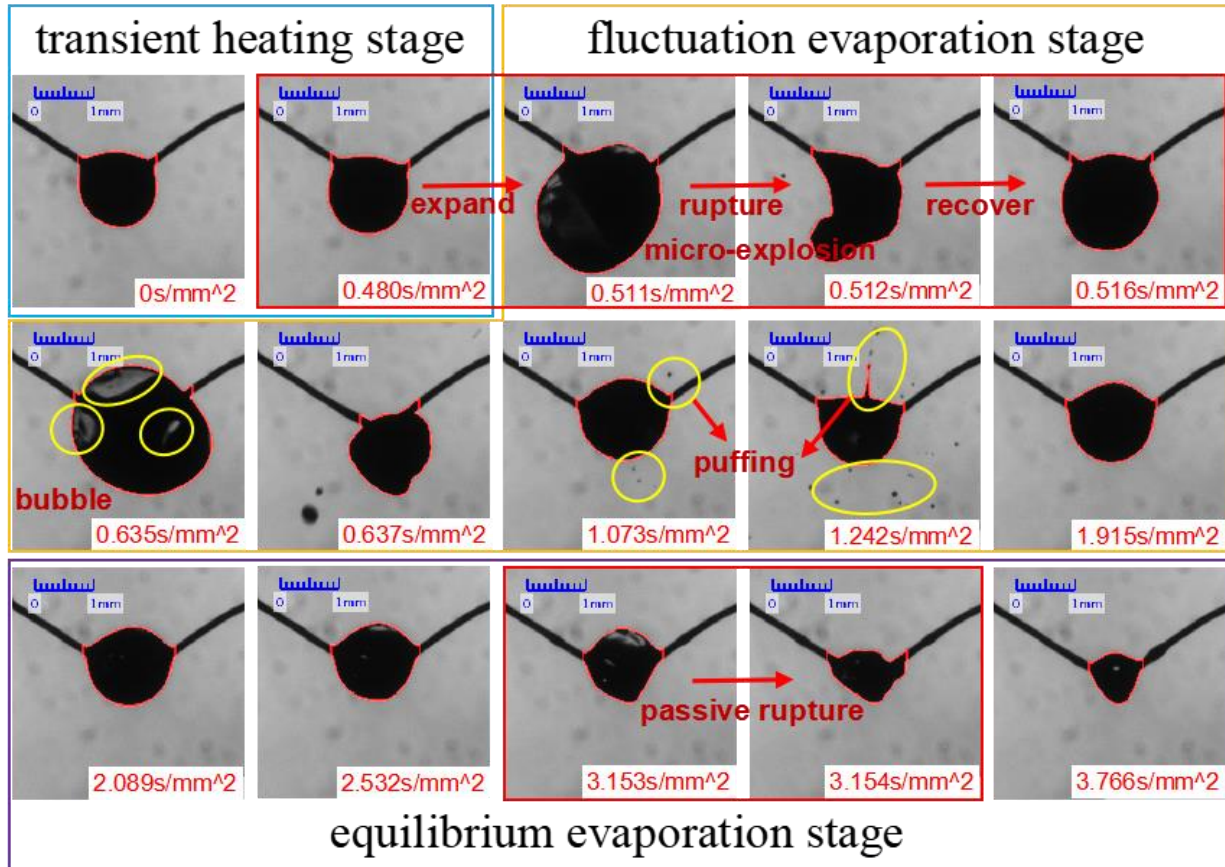


Fig. 5. Morphological changes during the evaporation of water emulsified diesel droplets at 673 K.

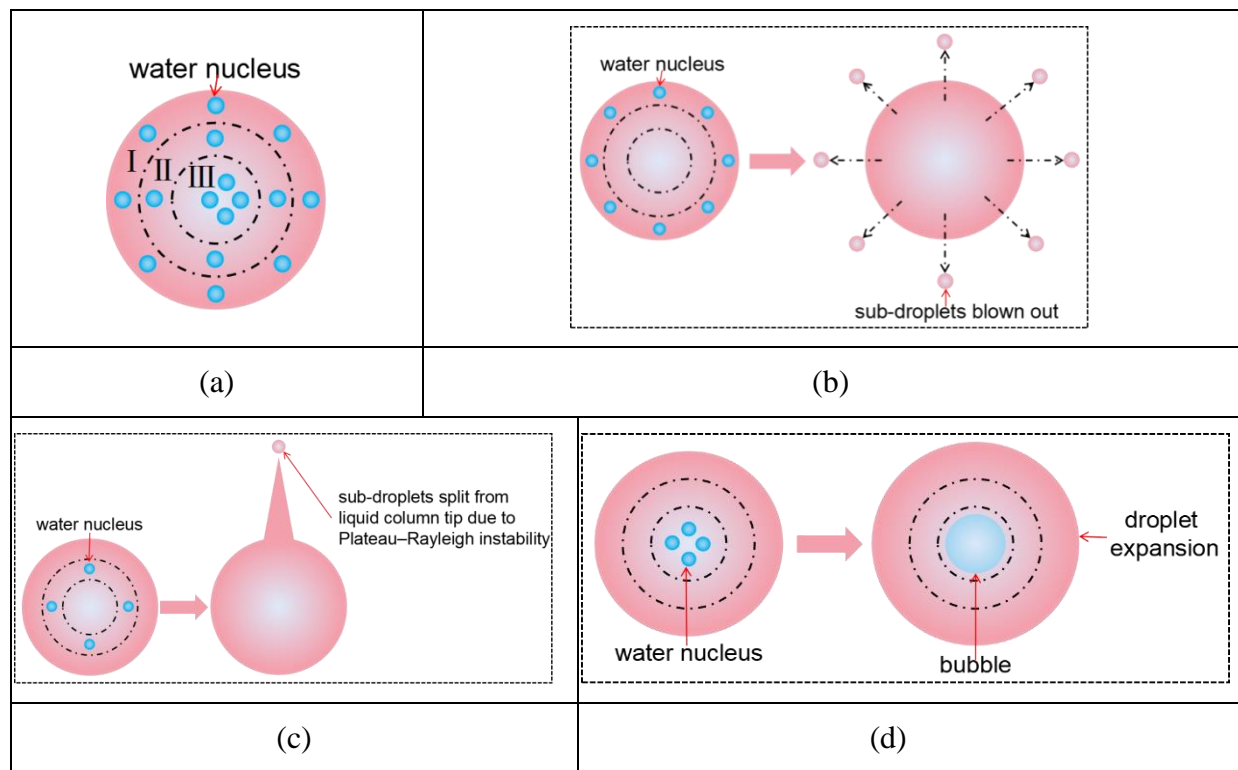


Fig. 6. Distribution and behaviors of water nuclei remained in droplet after micro-explosion: (a) distribution of water nuclei, (b) puffing caused by water nuclei in region I, (c) puffing caused by water nuclei in region II, (d) droplet expansion caused by water nuclei in region III.

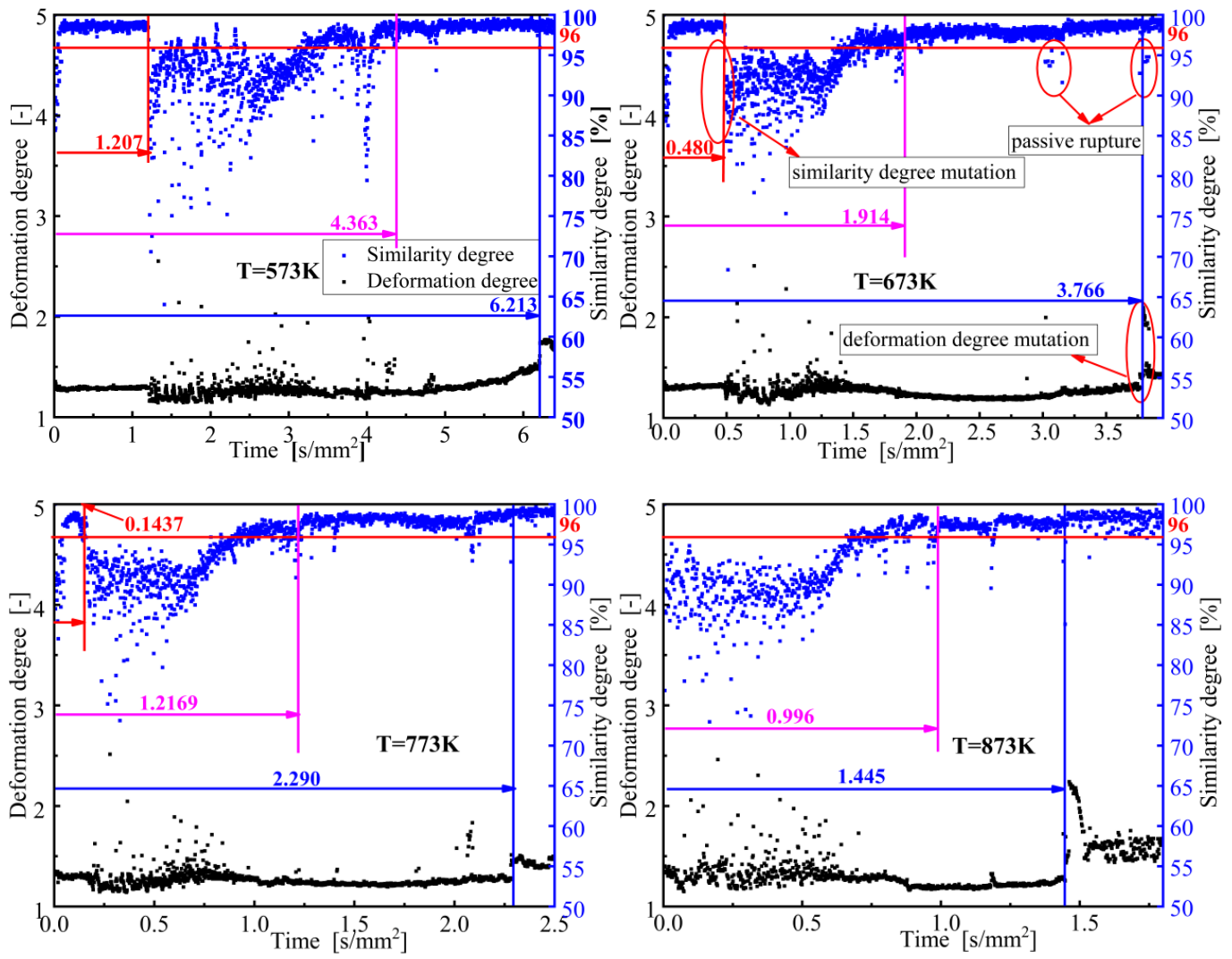


Fig. 7. The similarity and deformation degrees at different temperatures.



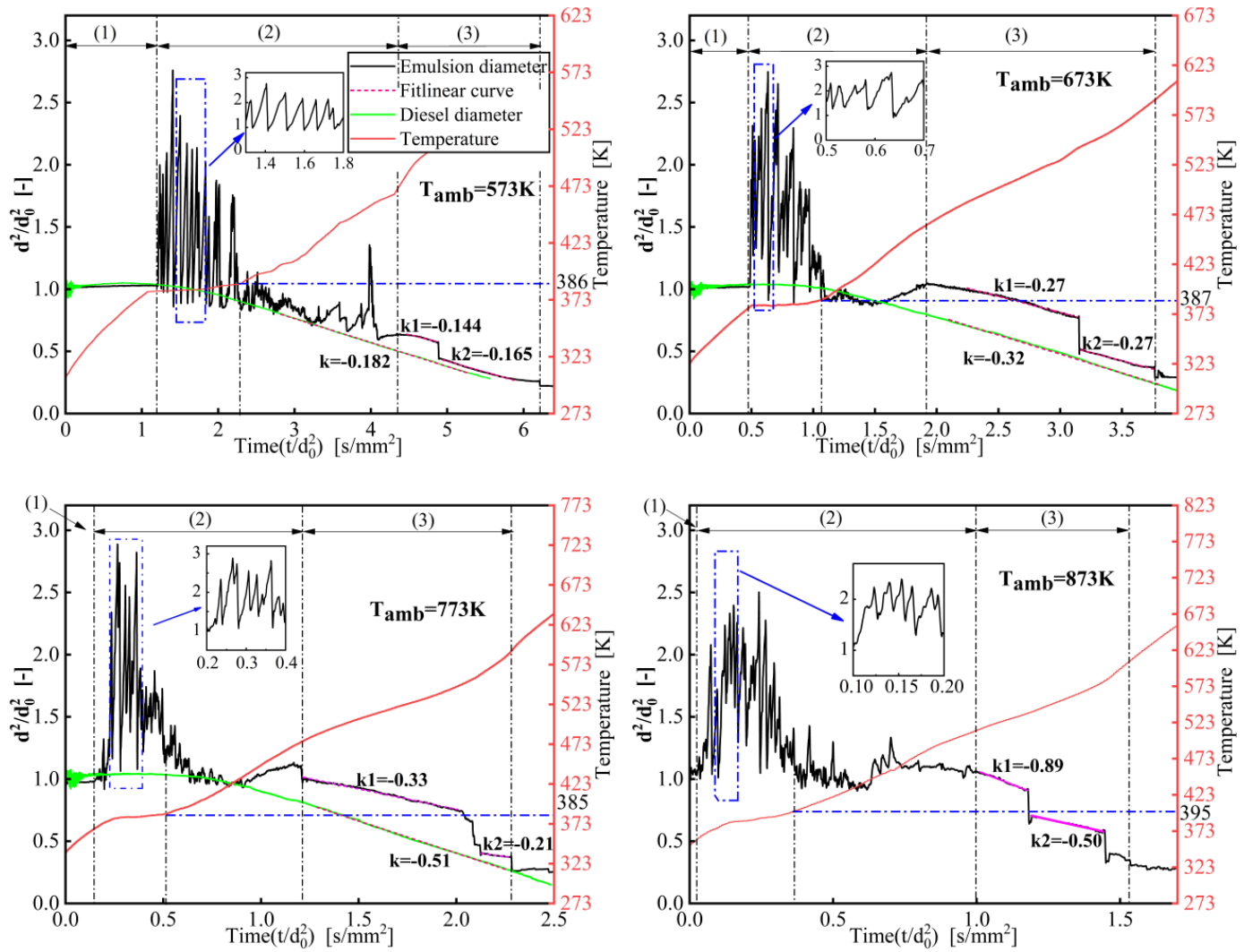


Fig. 8. Normalized squared diameter and droplet inner temperature at different ambient temperatures.

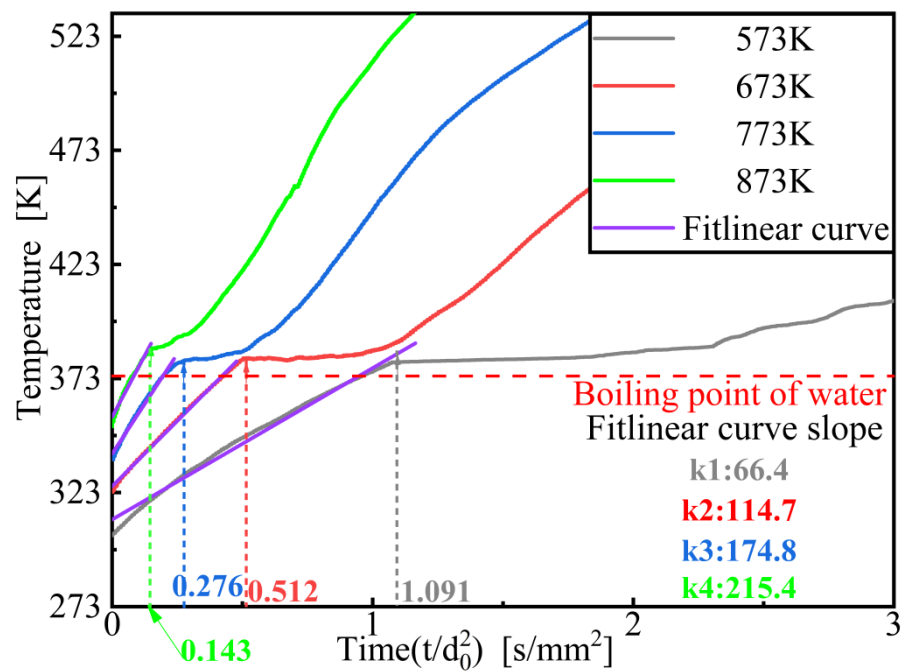


Fig. 9. Changes in droplet inner temperature.

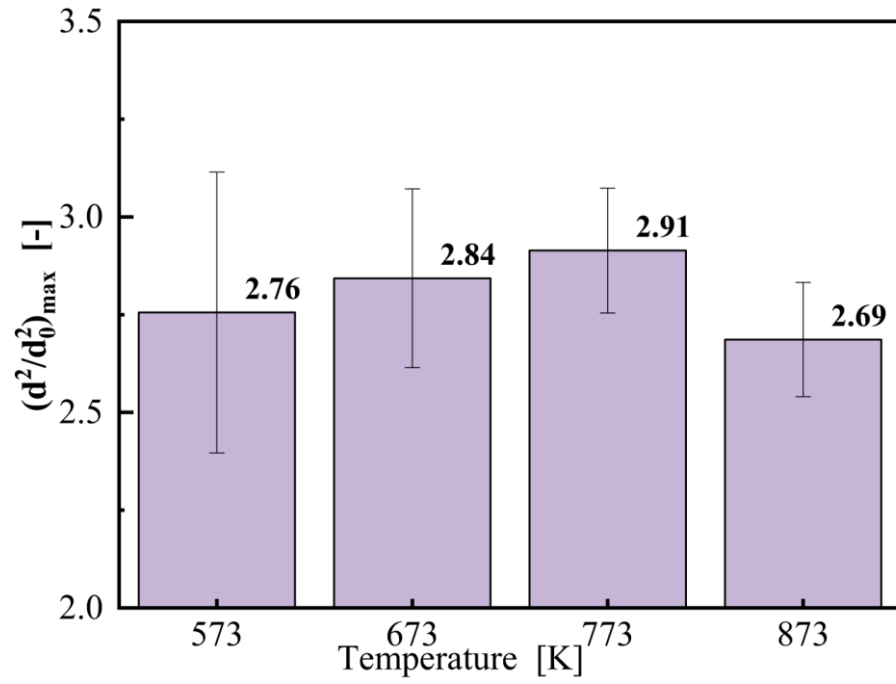


Fig. 10. Effect of ambient temperature on  $(d^2/d_0^2)_{\max}$ .

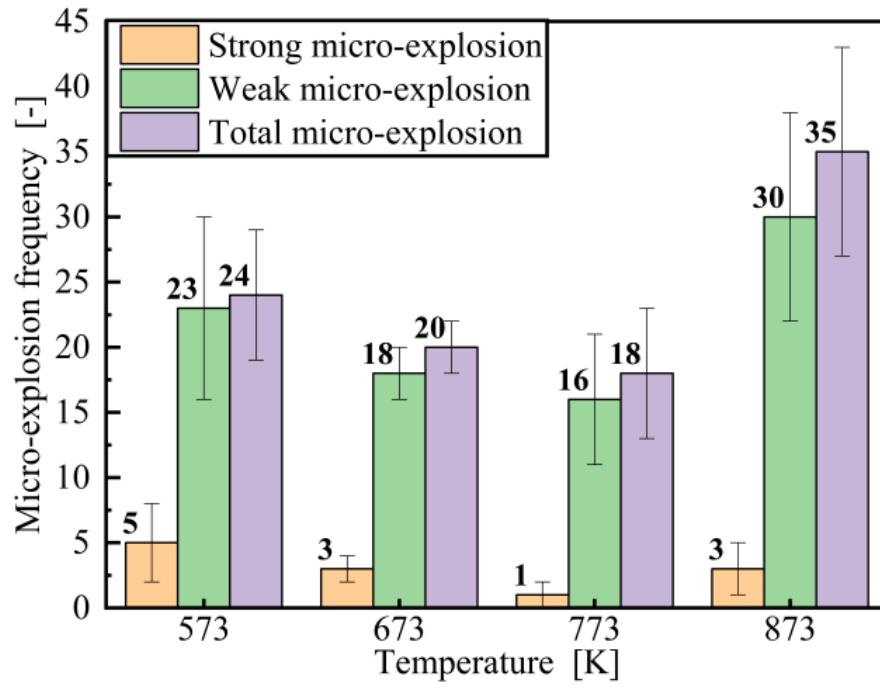


Fig. 11. Micro-explosion frequency.

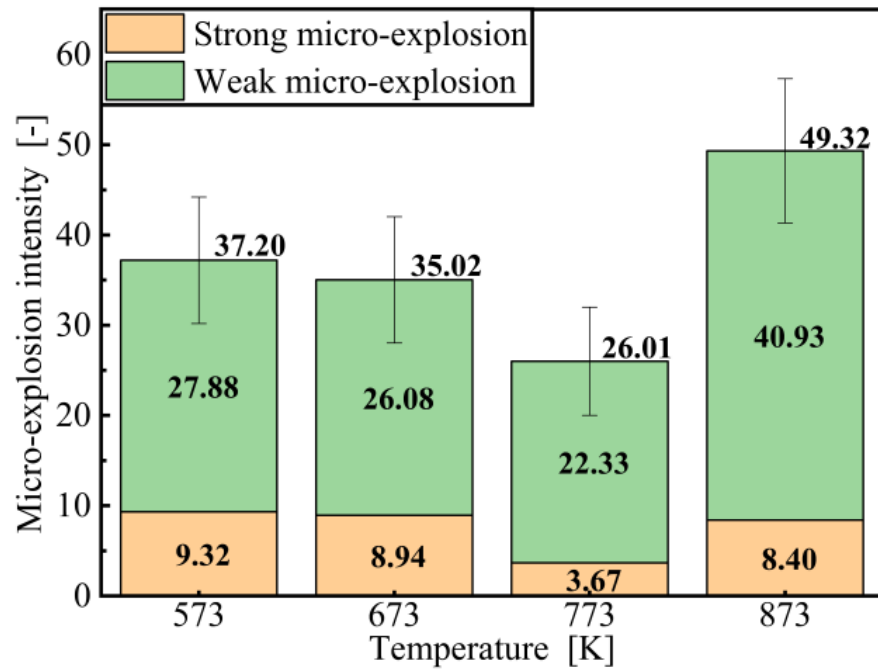


Fig. 12. Micro-explosion intensity.

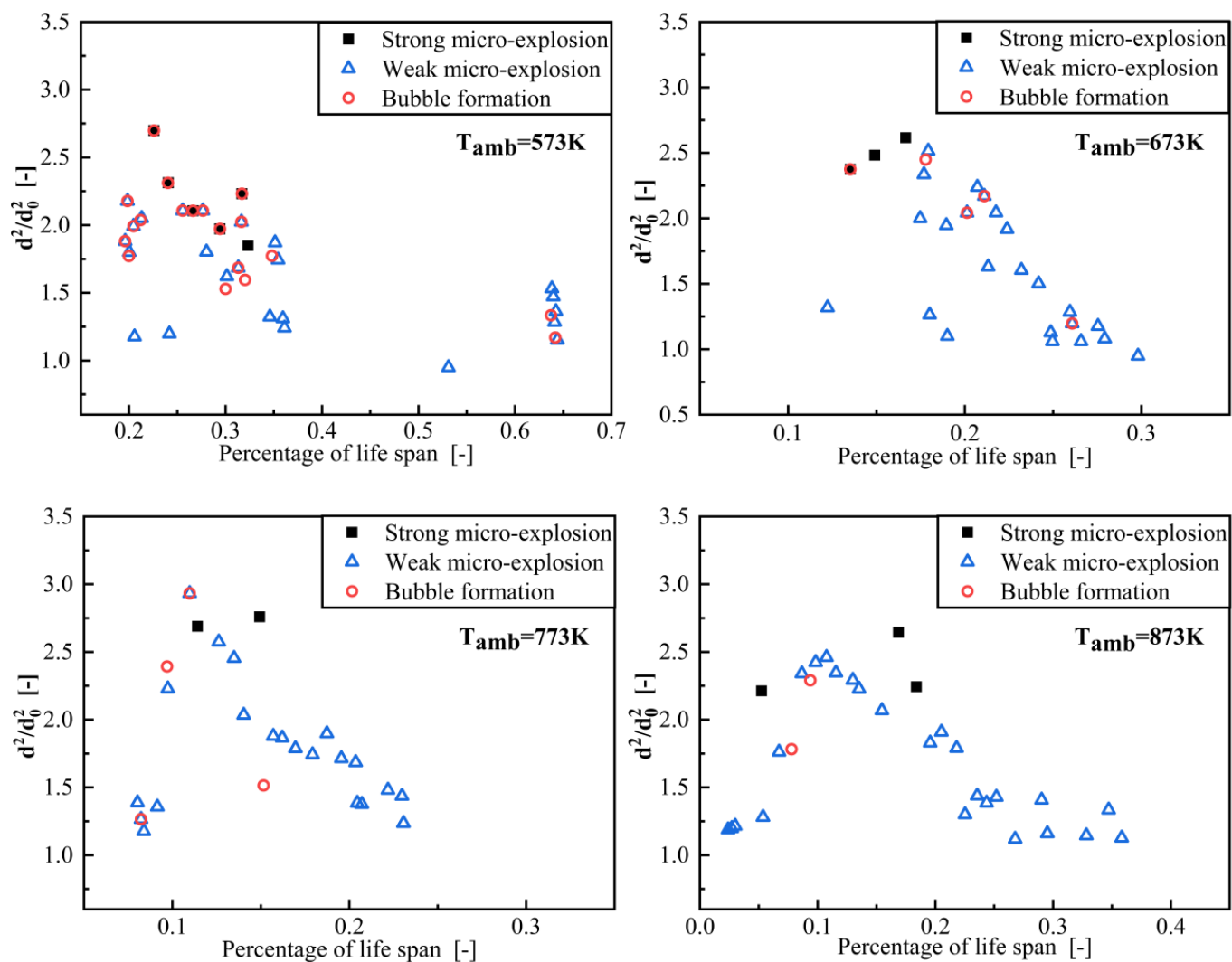


Fig. 13. Bubble formation and micro-explosion during evaporation of water emulsified diesel droplets.

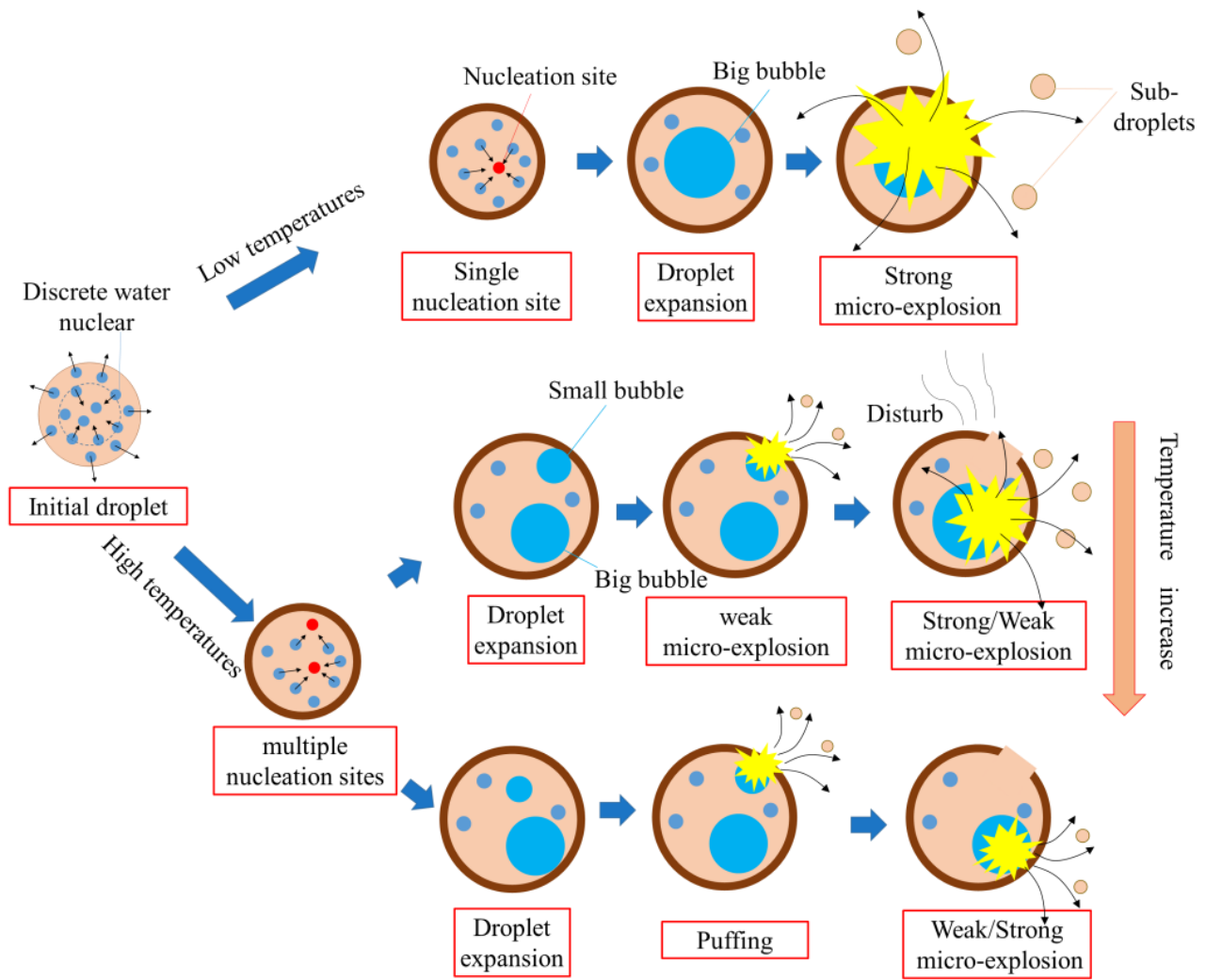


Fig. 14. Micro-explosion mechanism of water emulsified diesel droplets.

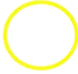

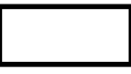

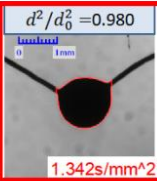
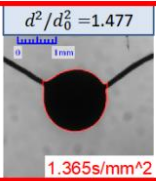
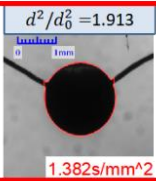
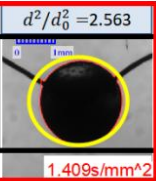
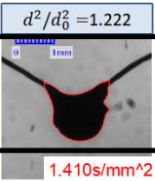
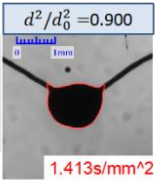
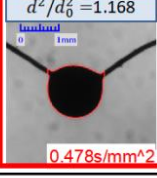
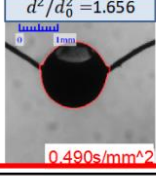
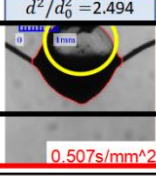
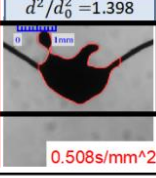
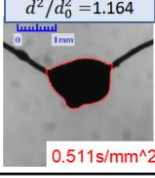
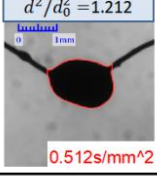
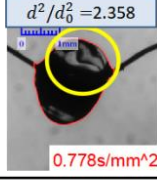
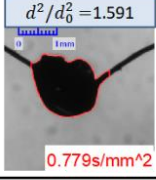
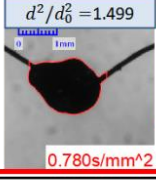
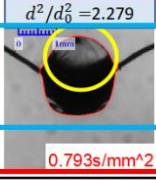
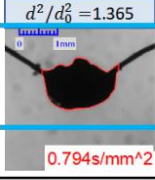
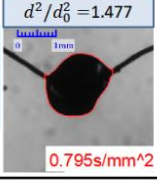
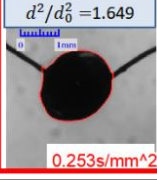
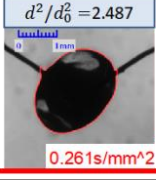
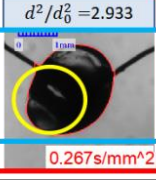
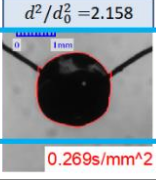
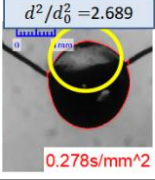
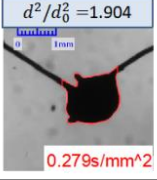
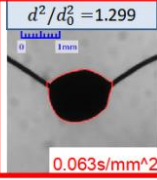
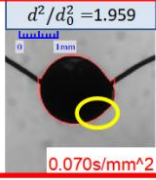
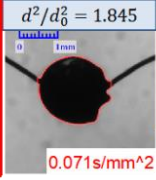
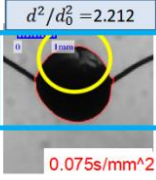
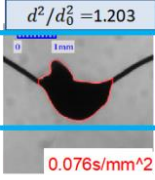
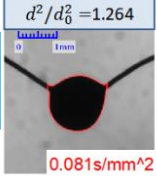
	 Droplet breakage position	 Bubble formation	 Strong micro-explosion	 Weak micro-explosion			
573K	Coincides with strong micro-explosion	 $d^2/d_0^2 = 0.980$ 1.342s/mm <sup>2</sup>	 $d^2/d_0^2 = 1.477$ 1.365s/mm <sup>2</sup>	 $d^2/d_0^2 = 1.913$ 1.382s/mm <sup>2</sup>	 $d^2/d_0^2 = 2.563$ 1.409s/mm <sup>2</sup>	 $d^2/d_0^2 = 1.222$ 1.410s/mm <sup>2</sup>	 $d^2/d_0^2 = 0.900$ 1.413s/mm <sup>2</sup>
673K	Coincides with strong micro-explosion	 $d^2/d_0^2 = 1.168$ 0.478s/mm <sup>2</sup>	 $d^2/d_0^2 = 1.656$ 0.490s/mm <sup>2</sup>	 $d^2/d_0^2 = 2.494$ 0.507s/mm <sup>2</sup>	 $d^2/d_0^2 = 1.398$ 0.508s/mm <sup>2</sup>	 $d^2/d_0^2 = 1.164$ 0.511s/mm <sup>2</sup>	 $d^2/d_0^2 = 1.212$ 0.512s/mm <sup>2</sup>
	Coincides with weak micro-explosion	 $d^2/d_0^2 = 2.358$ 0.778s/mm <sup>2</sup>	 $d^2/d_0^2 = 1.591$ 0.779s/mm <sup>2</sup>	 $d^2/d_0^2 = 1.499$ 0.780s/mm <sup>2</sup>	 $d^2/d_0^2 = 2.279$ 0.793s/mm <sup>2</sup>	 $d^2/d_0^2 = 1.365$ 0.794s/mm <sup>2</sup>	 $d^2/d_0^2 = 1.477$ 0.795s/mm <sup>2</sup>
773K	Coincides with weak micro-explosion	 $d^2/d_0^2 = 1.649$ 0.253s/mm <sup>2</sup>	 $d^2/d_0^2 = 2.487$ 0.261s/mm <sup>2</sup>	 $d^2/d_0^2 = 2.933$ 0.267s/mm <sup>2</sup>	 $d^2/d_0^2 = 2.158$ 0.269s/mm <sup>2</sup>	 $d^2/d_0^2 = 2.689$ 0.278s/mm <sup>2</sup>	 $d^2/d_0^2 = 1.904$ 0.279s/mm <sup>2</sup>
873K	Separation from strong and weak micro-explosion	 $d^2/d_0^2 = 1.299$ 0.063s/mm <sup>2</sup>	 $d^2/d_0^2 = 1.959$ 0.070s/mm <sup>2</sup>	 $d^2/d_0^2 = 1.845$ 0.071s/mm <sup>2</sup>	 $d^2/d_0^2 = 2.212$ 0.075s/mm <sup>2</sup>	 $d^2/d_0^2 = 1.203$ 0.076s/mm <sup>2</sup>	 $d^2/d_0^2 = 1.264$ 0.081s/mm <sup>2</sup>

Fig. 15. Droplet morphologies of micro-explosion and bubble formation.



Table 1. Experimental conditions.

Initial droplet diameter	0.8-1.2mm
Initial droplet temperature	298 K
Ambient temperature	573, 673, 773 and 873 K
Ambient pressure	101 kPa

Table 2. Variables and systematic errors.

Variables	Tool/method of measurement	Error
Ambient temperature	Thermocouple + PID controller	$\pm 5$ K
Response time	NI acquisition card	$\leq 10$ ms
Droplet diameter	High-speed CCD camera +MATLAB code	$\pm 1$ $\mu\text{m}$
Droplet inner temperature	K-type thermocouple	$\pm 1.1^\circ\text{C}$
Droplet volume	Microliter syringe	$\pm 0.5$ $\mu\text{L}$

Table 3. Classification criteria of micro-explosion intensity.

Micro-explosion classification	Classification criteria
Strong micro-explosion	$I > 2$
Weak micro-explosion	$1.2 < I < 2$
Puffing	$I < 1.2$